3-24-2016

Kinetics of higher lying Rb states after, Pulsed excitation of the D2 transition in the Presence of Helium

Austin J. Wallerstein

KINETICS OF HIGHER LYING RUBIDIUM STATES AFTER PULSED EXCITATION OF THE D_2 TRANSITION IN THE PRESENCE OF HELIUM

THESIS

Austin Jonathan Wallerstein, First Lieutenant, USAF

AFIT-ENP-MS-16-M-087

DEPARTMENT OF THE AIR FORCE
AIR UNIVERSITY

AIR FORCE INSTITUTE OF TECHNOLOGY

Wright-Patterson Air Force Base, Ohio

AFIT-ENP-MS-16-M-087

KINETICS OF HIGHER LYING RUBIDIUM STATES AFTER PULSED EXCITATION OF THE D_2 TRANSITION IN THE PRESENCE OF HELIUM

THESIS

Presented to the Faculty

Department of Engineering Physics

Graduate School of Engineering and Management

Air Force Institute of Technology

Air University

Air Education and Training Command

in Partial Fulfillment of the Requirements for the

Degree of Master of Science in Applied Physics

Austin Jonathan Wallerstein, B.S.

First Lieutenant, USAF

24 March 2016

AFIT-ENP-MS-16-M-087

KINETICS OF HIGHER LYING RUBIDIUM STATES AFTER PULSED EXCITATION OF THE D_2 TRANSITION IN THE PRESENCE OF HELIUM

THESIS

Austin Jonathan Wallerstein, B.S.
First Lieutenant, USAF

Committee Membership:

Dr. Glen Perram, PhD
Chair

Dr. Christopher Rice, PhD
Member

Dr. Charlton D. Lewis, PhD
Member

Abstract

The Diode Pumped Alkali Laser (DPAL) is a high power, three-level laser system that employs diode bars to optically excite an alkali metal vapor. It lases along the D_1 transition, between the two lowest energy levels, ${}^2P_{\frac{1}{2}}$ and ${}^2S_{\frac{1}{2}}$. Higher lying energy states are produced at higher population density via energy pooling and multiphoton processes. Pulsed laser excitation of rubidium at approximately 1 MW/cm^2 has been studied at helium pressure up to 900 Torr. Emissions from energy states as high as 82D suggests modest ionization, though these intensities decrease drastically at buffer gas pressures above 250 Torr. Blue emission from the $6^2P \rightarrow 5^2S_{\frac{1}{2}}$ transition and red emission from the $5^2D \rightarrow 5^2P$ transition indicate population in these upper states that persists at all helium pressures used in this experiment. A basic kinetic model was created to describe the concentration at these higher lying states. Optical trapping is severe at temperatures above 450 K. Diffusion of the rubidium is very slow, requiring mixing times exceed 45 minutes.

Acknowledgements

I would to thank Dr. Glen Perram for his guidance through this whole process, there were many times I could have gone done the wrong path, but he was always there to straighten me out. I'd also like to thank Dr. Chris Rice for his tireless efforts to helping me complete the experimental side. I knew I could always count on his assistance anytime I needed it. A thank you goes out to the lab technicians, Mr. Greg Smith and Mr. Mike Ranft. They were always the first person I turned to if I needed something in the lab, and they always seemed to have it. I'd also like to thank Lt. Josh Reding, who helped put me put all of this together in LaTeX and made sure it was perfect before it went in. Lastly, the obligatory thanking of my parents and family. Although they were not physically close, their presence was felt through this harrowing journey.

Austin Jonathan Wallerstein

Table of Contents

List of Figures

List of Tables

KINETICS OF HIGHER LYING RUBIDIUM STATES AFTER
PULSED EXCITATION OF THE D_2 TRANSITION
IN THE PRESENCE OF HELIUM

I. Introduction and Background

1.1 Introduction

The Diode Pumped Alkali Laser (DPAL) is a relatively new laser system that some believe may have the potential to become the next laser weapon system (15). The benefits of a DPAL are its scalable power and is able to keep excellent beam quality. However, there may be a few competing mechanisms to scale to higher powers, necessary to become a weapon system. One of those may be ionization. Ionization may limit the potential power that a DPAL is able to create or degrade efficiency at high pump intensity. This paper will investigate the kinetics in a laser pumped alkali and attempt to quantify the effect ionization in a pulsed DPAL laser systems. A kinetics model is presented in Chapter II without any ionization mechanism. Chapter **??** descirbes the experimental setup used for this invesitgation; the spectroscopic data is compared to the anayltic model in Chapter IV, and the omission of ionization is discussed. This thesis ends with a discussion of future experiments and model adjustments that can be done to better this investigation.

1.2 DPAL Laser

The first alkali laser demonstration occurred in 1962. Cesium vapor was excited to the $8^2P_{\frac{1}{2}}$ by an RF powered helium lamp, and it lased down to the $8^2S_{\frac{1}{2}}$ with a

wavelength of 7.18 μm (21). Following this demonstration, investigations into the emissions of the alkalies were undertaken, but their use as a laser system was shelved for many years after. This was mainly due to a lack of narrow band pump sources to allow for efficient pumping of the alkali. (29). It wasn't until late 2003 that a new alkali laser system was introduced when Dr. William Krupke secured a patent for the Diode Pumped Alkali Laser. This quasi-two level laser system utilizes the lowest three energy states of the alkali vapor—the ground state $n^2S_{\frac{1}{2}}$, and the first excited doublet $n^2P_{\frac{1}{2}}$ and $n^2P_{\frac{3}{2}}$, as well as a mixture of noble gases or specific molecular gases acting as a buffer. Technically three energy levels are used, but the higher two are so close in energy they can be equilibrated, hence "quasi-two level." The vapor is pumped along the D_2 transition line, $n^2S_{\frac{1}{2}} \rightarrow n^2P_{\frac{3}{2}}$, then, in the presence of the buffer gas, is collisionally relaxed to the slightly lower $n^2P_{\frac{1}{2}}$ state. From there the atom spontaneously relaxes to the ground state, emitting a near IR laser. Fig 1 shows this process in rubidium. The atom is excited along the D_2 transition, 780.0259 nm, from $5^2S_{\frac{1}{2}}$ to $5^2P_{\frac{3}{2}}$. Through spin-orbit mixing, the atom relaxes to the $5^2P_{\frac{1}{2}}$ and then lases back to the ground state along the D_1 transition, 794.7596 nm (15).

Some of the fundamental qualities of the DPAL lend themselves very well to in depth study and development. Due to the size of the spin orbit splitting–at most 555 cm^{-1}–alkali lasers have an extremely high quantum efficiency compared to their solid state counterparts (16). The DPAL's quantum efficiency is over 95% , compared to around 85% for Nd:YAG lasers (9) and 80% for Ti:Sapphire systems (1). Secondly, this laser system utilizes a gaseous vapor as its gain medium, giving rise to other promising features of the DPAL system, namely lower thermal aberrations and easier scalability to extremely high powers. Thermal effects in solid state lasers can cause unwanted stress on the lasing medium, leading to degradation in beam quality. Stresses on solid state lasing media can created subtle modifications to the index of

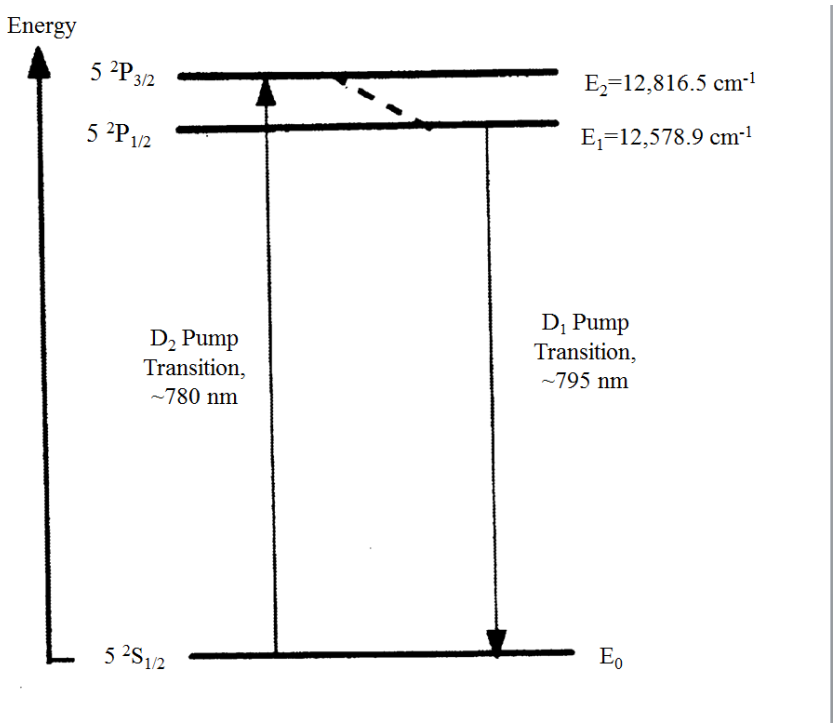

Figure 1. The three lowest levels in an alkali atom. The spin orbit relaxation occurs only in the presence of buffer gas, as the density of alkali atoms make the spin orbit mixing rate very low.

refraction, creating phase changes of a beam passing through and degrading the quality of the beam (8). In gas lasers, the medium can flow through the cavity reducing this issue by cycling in cooler vapor and not allowing temperature to accumulate. The DPAL system also has an easy way to scale up to higher powers. Power can easily be produced in a DPAL by increasing pump intensity and carefully increasing volume.

Both of these issues have been investigated at length. R. Beach *et al.* (6) have investigated both the theoretical thermal effects and the power scaling advantages of DPAL laser systems over their solid state counterparts. They demonstrate that the two leading causes for thermal aberrations of the laser are thermal conductivity of the gain medium and its refractive index's dependence on temperature. Less thermal conduction means less pump power is lost through heat, and a smaller index dependence

on temperature implies better beam quality. The DPAL system outperforms solid state lasers in both of these metrics. The DPAL is 67 times less thermally conductive than the typical solid state lasers, and has a gain medium that gets has an index of refraction that is less temperature dependent than solid state lasers. They also discuss a theoretical geometry for convectively cooling a flowing gas, and conclude that the laser efficiencies would be higher with an alkali based system.

W. Krupke (16) expands on the possibility of scaling the power of the DPAL laser, suggesting that the way forward is to pump these lasers transversely, as opposed to longitudinally. In a longitudinal pumped geometry, the pump beam runs parallel to the output beam, whereas in the transversely pumped scheme, the pump beams comes perpendicular to the direction of the output beam. In static non-flowing systems, this geometry allows for an increase in the pump power insertion area, while maintaining reasonable temperature gradients. Using this geometry, peak laser power was more than doubled compared to the end pumped design, 49 W from 13 W. Krupke further discusses geometries for flowing the alkali vapor, in a triply transverse device. Here the gas flows perpendicular to both the pump beams and the output laser. Using this geometry a device was shown to produce power considerably higher than that of the static non-flowing device, 130 kW in a quasi-CW output beam, when pumped with 63mJ.

Although the DPAL seems much more scalable than solid state lasers, there still remain issues for reaching the maximum power output in these systems. At high pump power, there is an apparent decrease in output laser power as you scale input power. Above 70W of CW pump power, the output power falls off, dropping from 20W output with 70W pump to 15W out at 100W pump intensity (19). Many different theories have been posited as to explain this phenomenon.

The first of these is alkali-buffer gas chemical reactions. The buffer gas in the

lasing medium is a mixture of rare gases, like helium, and specific hydrocarbons, such as ethane or methane. The hydrocarbons have a much larger spin-mixing rate that rare gases but undergo chemical reactions that significantly degrade laser power. A modeling of a cesium laser, with a hydrocarbon density of 1/5 the helium density, exhibits a 75% drop in the output power when chemical reactions are taken into account (5). For this reason, a buffer gas consisting of pure helium is preferable, but the spin orbit mixing cross sections is too small for this to be a practical scenario, especially in the larger elements. A purely helium buffer works for potassium, but the helium pressure needed to create the same stimulated emission rate in cesium is 230,000 atm (16).

The next deleterious process is thermal lensing. While the effects are not as serious in the DPAL laser as in the solid state laser, they still exist must be considered. Thermal lensing can occur when the index of refraction of the gain media changes enough to cause a quarter wave distortion. This has been shown to cause distortions in the lasing cavity, causing beam degradation at realistic temperatures. Laser decay time falls from 4.5 ms to 0.5 ms as the cell temperature is increased from $165°C$ to $200°C$ (30).

The third and most intriguing challenge to scaling power in the DPAL system is that of ionization. The first two issues seem to have simple, albeit incomplete, solutions; rubidium can used in an all helium environment to avoid chemical reactions, and convective flow can be utilized to mitigate the thermal aberrations—a modest flow of 7 m/s in the direction of the pump beam has been shown to mitigate the thermal lensing problem (30). Ionization, though, seems to occur with all of the alkalies and a solution is not immediately apparent (13). When an alkali atom is ionized, its electron can no longer cycle through the process necessary for lasing to occur. If a sufficient density becomes ionized, there will less atoms available for lasing.

The rates of photoionization have been shown to be significant, on the order of $\frac{10^3}{sec}$ in situations with extremely high buffer gas pressures. Theoretically it would be possible to use a convective flow to cycle new atoms into the laser gain area to alleviate this problem, however it would require nearly supersonic flows to remedy the situation (13).

What makes this problem of photoionization so vexing is the fact that while the effects have been shown experimentally (10), there is no obvious mechanism for this process to occur. In all of the alkalies, there are no energy levels accessible with a photon from the pump source, except the doublet P that is being purposefully excited; and the pump photon does not have enough power to cause ionization from that first excited state. A single pump photon can ionize an atom from a doubly excited state, so it is likely that some mechanism is creating population at higher energy levels.

The two leading theories in this matter are energy pooling and off-resonant excitation into the wings of the absorption line shape (19). Energy pooling occurs when two singly excited rubidium atoms collide to create a doubly excited atom and one in the ground state, $Rb^* + Rb^* \rightarrow Rb^{**} + Rb$. Here, Rb* represents an atom with an electron in either of the 5P states, Rb is an atom with its electron in the 5S state, and Rb** is the doubly excited atom (12). The second mechanism involves the buffer gas broadening the line width of a double excited, such that a pump photon can excite an electron in the first excited doublet, or from the ground state, to this doubly excited state with a two photon process. In both cases the the primary states excited by this mechanism are the $(n+2)^2S$ and the n^2D states—where n is the ground state quantum number for the specific alkali (12; 13). Recall, for rubidium the 5^2S state is the ground state, so the 7^2S and 5^2D states are the primary states created by these two mechanisms.

There exists mechanisms of ionization other than single photon photoionization preciously discussed. Just as a two photon process can create a doubly excited atom, two photon processes can create an ion from a singly excited alkali atom (4). Penning ionization can occur when, similar to energy pooling, an excited alkali atom collides with another to impart energy. This time, though, a singly excited atom collides with a doubly excited atom, creating a ground state atom, an ion, and a free electron. The other mechanism is associative ionization processes, in which two singly excited atoms collide and bond, creating an excited alkali dimer and a free electron (17).

There is some evidence that ionization may not have that serious of an effect the DPAL. Sulham *et. al* found linear scaling of the DPAL up to 32 times the threshold value, 43 kW/cm^2 pump intensity, in pulsed experiments. They were able to scale up the DPAL without seeing these secondary effects (23). Hurd *et. al* found that secondary mechanisms, including ionization, only had a minor effect for a potassium laser pumped by pulses with 7 MW/cm^2 (11). It could be that the mechanisms for producing ions are not fast enough processes or that at the high buffer gas pressures that are required, the recombination rate is such that any ion that is produced will immediately recapture an electron and re-enter the DPAL cycle. The general disagreement in the scientific community makes this problem more interesting and this research more important.

There are a few other complications that must be identified with this laser. The first of which is the possibility of creating stimulated emission at unexpected wavelengths, through two-photon absorption. It has been shown that through a two photon process, a ground state electron can be excited to a highly excited D state. The photon then can lase in the infrared down to a neighboring P state, and lases again in the blue back down to the ground state. In rubidium, the ground state electron, in $5^2S_{\frac{1}{2}}$ is excited using a pump beam at 778.1 nm to the $5^2D_{\frac{3}{2}}$ state. It then

lases at around 3 μm to the 6P manifold, where it lases again to the ground state at 420.2 nm (24). Note that the traditional rubidium DPAL laser lases from the 5P manifold. Care is needed to not accidentally excite this two-photon process, because two pump wavelengths differ by less than 2 nm. Ionization is much more accessible at this higher energy level.

The other major difficulty of making a DPAL is a phenomenon called radiation trapping. This occurs when radiation is emitted by an atom and that radiation is reabsorbed by another atom before it can reach the detector. This cycle of emission and reasorption can occur many times over the path from the original emission to reaching the detector. The effect of this trapping will be a perceived increase in the observed lifetime of a state (28). The magnitude of this phenomenon are a function of a few variables, including number density of the lower state, absorption cross section (and therefore line shape) and experimental geometry. Molisch and Oehry go into fantastic detail in (18), and conclude the normalized eigenmodes of the Holstein equation analytically solve this problem. Such detail is not taken presently, but it must be considered during any analysis.

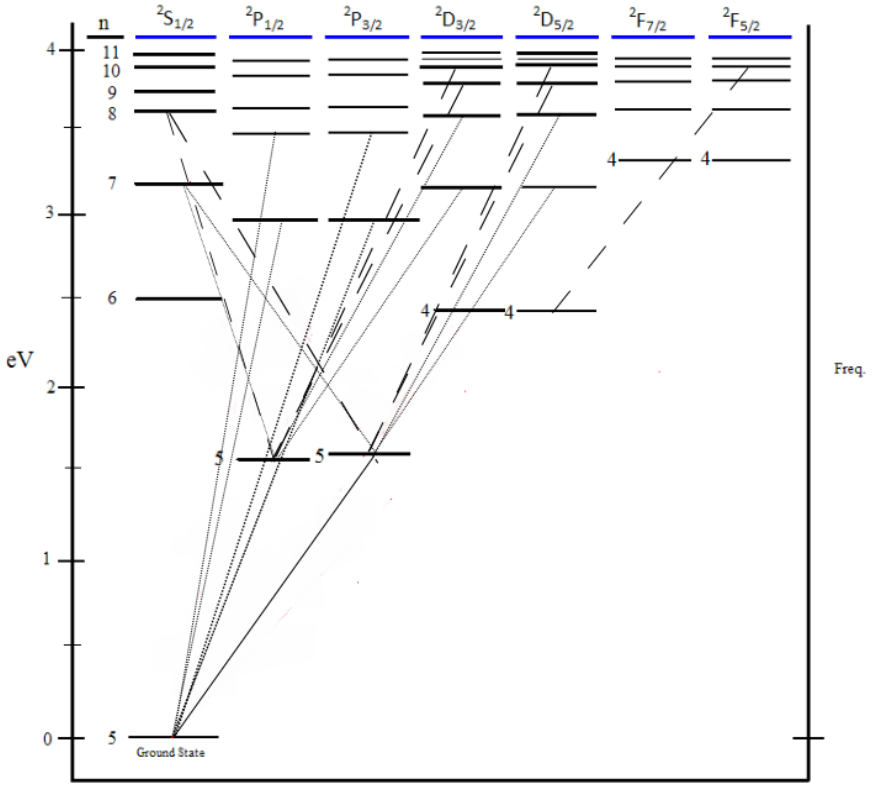

Figure 2. The Grotian energy diagram for Rubidium. There exist many more dipole allowed transitions in both the UV and IR spectrum, but this paper will focus only on the primary visible and NIR transitions, here represented by the dotted lines.

1.3 Rubidium

All of these issues are valid for the alkalies. This investigation focuses solely on rubidium. In this case the ground state is the $5^2S_{\frac{1}{2}}$ and is pumped along the D_2 line centered at 780.0268 nm to the 5^2P doublet, and lases along the D_1 line centered at 794.7603 nm (14). Figure 2 shows the different energy levels of rubidium. The D_2 pump line the solid line, the most prominent transitions in the visible and near infrared spectrum are shown in dotted, and other major dipole allowed transitions are represented by the dashed lines.

The transitions monitored in this experiment are annotated in Table 1. The first

column is the vacuum wavelength of the emitted light. The second column is the atomic transition that emits the specific photon, written as the lower state level nl_j, then the upper state (14). The last two columns are Einstein A coefficients for the transition; if it is available in the National Institute of Standards and Technology (NIST) Atomic Spectra Database, it is quoted in the third column. The final column is an analytic estimation of the A coefficient found using a hydrogenic approximation (20). As a note, for all the analysis done, the NIST database A coefficient was used when it existed, for all others, the Payling number was used.

The model that is created in the next section examines the primary doubly excited states and suggests a method for creation of them based on some mechanisms identified in this Chapter, specifically energy pooling. This model can be compared to spectroscopic intensities of the tranisition lines from Table 1 and an estimation of the model's validity can be made.

Table 1. Rubidium atomic transitions. If a transition has no A-coefficient quoted in the NIST database, the entry will be blank.

λ (in nm)	Transitions (Lower, Upper)	NIST (in 10^8 sec^{-1})	Payling (in 10^8 sec^{-1})
358.7050	$5S_{\frac{1}{2}}, 7P_{\frac{3}{2}}$	0.0040	0.0040
359.1572	$5S_{\frac{1}{2}}, 7P_{\frac{1}{2}}$	0.0029	0.0029
420.1788	$5S_{\frac{1}{2}}, 6P_{\frac{3}{2}}$	0.0177	0.0180
421.5519	$5S_{\frac{1}{2}}, 6P_{\frac{3}{2}}$	0.0150	0.0150
564.7761	$5P_{\frac{1}{2}}, 7D_{\frac{3}{2}}$		0.0150
572.4106	$5P_{\frac{3}{2}}, 7D_{\frac{5}{2}}$		0.0190
607.0746	$5P_{\frac{1}{2}}, 8S_{\frac{1}{2}}$		0.0086
615.9619	$5P_{\frac{3}{2}}, 8S_{\frac{1}{2}}$		0.0160
620.6305	$5P_{\frac{1}{2}}, 6D_{\frac{3}{2}}$	0.0295	0.0250
629.8324	$5P_{\frac{3}{2}}, 6D_{\frac{5}{2}}$	0.0371	0.0310
727.9989	$5P_{\frac{1}{2}}, 7S_{\frac{1}{2}}$		0.0180
740.8166	$5P_{\frac{3}{2}}, 7S_{\frac{1}{2}}$		0.0350
761.8925	$5P_{\frac{1}{2}}, 5D_{\frac{3}{2}}$		0.0410
775.7647	$5P_{\frac{3}{2}}, 5D_{\frac{5}{2}}$		0.0530
780.0259	$5S_{\frac{1}{2}}, 5P_{\frac{3}{2}}$	0.3861	0.3700
794.7596	$5S_{\frac{1}{2}}, 5P_{\frac{1}{2}}$	0.3610	0.3400

II. Model

This chapter will outline a simplified model that can be used to describe the kinetics of the DPAL system. It is not presented as a complete model that accounts for all of the possible mechanisms occurring in rubidium, it is simply one possibility. The mechanisms chosen are believed to be the dominant mechanisms in this process. But ionization is purposefully neglected. If this model is able to correctly predict the data, then it suggests that ionization may not be a major factor in the kinetics. If the model is insufficient, though, then ionization remains a possiblity.

This model requires a few major assumptions. First, it is assumed that the pump intensity is much greater than the saturation intensity all the way through the cell. This is a fair assumption as the pump intensity being used is approximately 10^6 times that of the saturation intensity, so the D_2 transition is bleached for the entire laser line. The next assumption is that the radiation trapping acts solely by decreasing the A coefficient, effectively increasing the decay rate. The trapping factor can be described as a probability that a given photon will be able to escape the cell, and it is modelled as function that goes from 0 to 1 and is dependent on rubidium number density and buffer gas number density only. Radiation trapping's dependence on the buffer gas manifests itself through the line shape and therefore the absorption corr-section. All other dependencies are neglected, including geometry, as they remain constant through the experiment.

The third assumption is the total population of rubidium atoms are in the ground state and the first excited manifold, the $5^2P_{\frac{3}{2}}$ and $5^2P_{\frac{1}{2}}$ states. This is a valid assumption as the data will reveal later in Chapter IV. The density in states excited above the 5^2P states is two or three orders of magnitude less than the density in those states, so we can neglect them in the total rubidium density. Furthermore, the only other states that have any contribution to the overall density are the 6^2P and 5^2D

manifolds. These two are the only states not included in the lasing process that emit enough light to be seen in experimental results under all conditions. The final assumption is a bit more difficult. It is assumed that there exists no radial dependence on the output of the rubidium sample, that is to say everywhere in the pump beam is pumped equally. This is done to simplify some of the calculations; attempting to account for this would be mathematically difficult. Everywhere in the pump spot does not have the same power though; there exists some distance from the center of the spot where the pump power has fallen past the saturation intensity. At this point the excited rubidium density will drop significantly. To counter this, much of the experimentation is done at approximately the same pump power, near 8 MW/cm^2, so that the bleached volume stays relatively constant and the effects of this density gradient will be the same over all of the runs. This does not solve the problem, but does allow for the effects to be negated as they should remain constant during the course of the experiments.

The only kinetic reactions considered in the model are laser pumping, spin orbit mixing, energy pooling, spontaneous emission and quenching. They represent the main processes of energy transfer in the cell and will hopefully be able to correctly predict the data. The first process is the excitation of the rubidium along the D_2 resonance transition by the pump laser:

$$N_0 + h\nu_p \rightarrow N_2 \tag{1}$$

Here, N_0 is a rubidium atom in the ground state, N_2 is one in the $5^2P_{\frac{3}{2}}$ state, and $h\nu_p$ describes a pump photon at 780.0 nm. The next reaction is the spin orbit mixing of the 5^2P manifold with the buffer gas:

$$N_2 + He \overset{k_{21,12}}{\leftrightarrow} N_1 + He \tag{2}$$

Now N_1 and M are introduced; N_1 is a rubidium atom in the slightly lower $5^2P_{\frac{1}{2}}$ level and M is a atom of the buffer gas, in this case helium. The rate coefficients k_{21} and k_{12} are the forward and backward fine structure mixing of Eq. 2, respectively. The next reaction is the energy pooling of singly excited atoms to a doubly excited one:

$$N_{1,2} + N_{1,2} \overset{k_{p3,p4}}{\rightarrow} N_{3,4} + N_0 \tag{3}$$

On the left side of Eq. 3, $N_{1,2}$ refers to either an electron in the $5^2P_{\frac{3}{2}}$ or $5^2P_{\frac{1}{2}}$ states. This model does not make a distinction between the two singly excited states concerning pooling. This is not technically correct, as the different spin-orbit splitting does result in different pooling rates (12), but the values are close enough to be assumed equal for this work. On the right side of that equation, $N_{3,4}$ refers to either a rubidium atom with an excited electron in the 5^2D manifold, or the 6^2P manifold, respectively. Due to the distribution of the excitation, both states in the manifold will be included. The rate at which these reactions occur will be k_{p3} and k_{p4}, with k_{p3} referring to the $5D$ process and k_{p4} referring to the other. These first processes are the primary mechanisms for creation of the excited atoms, the next equations will describe the relaxation. The first of these is spontaneous emission.

$$N_i \rightarrow N_j + h\nu_{ij} \tag{4}$$

In this equation, N_i can refer to any of the four excited states, acting as the upper state in the transition, and N_j will be the lower state and can be either the ground state or the 5P manifold (i.e. $j = 0, 1, 2$). Also, $h\nu_{ij}$ is the photon emitted at the wavelength corresponding to the transition. The rate at which these reactions occur is the A-cofficeint associated with the transition, in $\frac{1}{sec}$. The final process is quenching. Recall, in this process, an excited electron is collisionally relaxed to a lower energy

manifold.

$$N_{3,4} + He \overset{k_{q3,q4}}{\rightarrow} N_j + He \tag{5}$$

The N_j in this equation refers to any other energy state lower in energy than the initial state. So from the 6^2P manifold, the electron can be quenched to the ground or the 5^2P state, but not the $5D$. From the 5^2D state, though, it can quench to any of the states that have been discussed thus far. The rates that these processes occur will be k_{q3} and k_{q4}, again referring to the process of N_3 and N_4 respectively.

Using these processes, rate equations can be derived. For the rest of the analysis, n_j will be the number density of the the j^{th} state, and m will be the helium density, [He]. The states will be denoted similarly to the process equations, where n_0 is the ground state density, n_1 is the density in $5^2P_{\frac{1}{2}}$, n_2 is the density in $5^2P_{\frac{3}{2}}$, n_3 is from the total 5^2D manifold, both $5^2D_{\frac{5}{2}}$ and 5^2D_32, and n_4 is the density in the entire 6^2P manifold, both the $6^2P_{\frac{3}{2}}$ and $6^2P_{\frac{1}{2}}$. The un-sub-scripted variable n will be the total rubidium density.

To start, the rate equation for the D_2 transition is writted:

$$\frac{dn_2}{dt} = \frac{\sigma_{02}}{h\nu_p} I_p(n_0 - \frac{1}{2}n_2) - \xi_2 A_2 n_2 - k_{21} m n_2 + k_{12} m n_1 \tag{6}$$

where σ_{02} is the absorption cross section of this transition, I_p is the intensity of the pump beam and ξ_2 is the resonance trapping of the D_2 transition. The symbol ξ represents the radiation trapping factor, and the subscript associated with the the symbol will represent the states as described above. The terms relating to the processes that are not included in this rate equation, specifically the pooling and the quenching are able to be neglected because of the first major assumption that was made. The number densities in the higher excited states are negligible to the those in

the lower excited states, so the contribution to and removal of n_2 due to the creation and destruction of those states must be negligible.

The first term in Eq. 6 is known as the pump rate:

$$R_p = \frac{\sigma_{02}}{h\nu_p} I_p (n_0 - \frac{1}{2} n_2) = \frac{I_p}{I_s} A_2 (n_0 - \frac{1}{2} n_2)$$

where $I_s = \frac{h\nu_p A_2}{\sigma_{02}}$ is the saturation intensity of the sample. This must be a finite rate, and because we assumed that the entire cell was bleached, $I_P >> I_s$, it is required that $n_0 - \frac{1}{2} n_2 \to 0$, or

$$2n_0 = n_2 \tag{7}$$

The other term in Eq. 6 that requires more thought is the trapping factor. The only requirement that must be met is that it be a function that ranges from 0 to 1–with 0 being the most trapped–and goes down as n goes up. If there was minimal rubidium in the cell, there would be no trapping, and $\xi = 1$. A pragmatic, but not theoretically supported, functional form for trapping is proposed:

$$\xi = \frac{1}{(1 + bn)^k} \tag{8}$$

The constants b and k may be functions of absorption cross section, so they can be variable for different transitions and buffer gas pressure. This will be discussed in much more depth in Chapter IV of this thesis.

Turning back to Eq. 6, to investigate the value of n_2, a steady state solution must be found. To achieve this, the function is integrated over all time, which is equivalent to setting the time rate of change equal to 0 (For a secondary discussion of this step, considering the Boltzmann equation, see Appendix B). Setting Eq. 6 equal to 0, and invoking an assumption from above, such that $n = n_0 + n_1 + n_2$:

$$\frac{I_p}{I_s}A_2(n - n_1 - 3/2n_2) + k_{12}mn_1 = (\xi_2 A_2 + k_{21}m)n_2 \tag{9}$$

In order to solve for n_2 solely as a function of n, the rate equation for n_1 must be examined, it is written:

$$\frac{dn_1}{dt} = k_{21}mn_2 - k_{12}mn_1 - \xi_1 A_1 n_1 = 0 \tag{10}$$

$$n_1 = \frac{k_{21}m}{k_{12}m + \xi_1 A_1} n_2 = \gamma n_2 \tag{11}$$

where γ is the parameters in front of n_2 in Eq. 11, specifically $\gamma = \frac{k_{21}m}{k_{12}m+\xi_1 A_1}$. Plugging this value back into Eq. 9:

$$\frac{n_2}{n} = \frac{\frac{I_p}{I_S}A_2}{\frac{I_p}{I_s}A_2(\frac{3}{2} + \gamma) + (\xi_2 A_2 + k_{21}m - k_{12}m\gamma)} \tag{12}$$

Because $\frac{I_p}{I_s} >> 1$ Eqs. 10 and 12 can be simplified to:

$$n_2 = \frac{1}{\frac{3}{2} + \gamma} n \tag{13}$$

$$n_1 = \frac{1}{1 + \frac{3}{2}\frac{1}{\gamma}} n \tag{14}$$

Obviously, as a function of total rubidium density, in the absence of any trapping, you would expect the excited state density to increase as well, which is what the model predicts. The effect of trapping is less obvious and will be discussed later. The helium dependence of these can be easily seen in γ. As a function of helium density, γ starts very close to 0 and rises approximately to 1. So at $m = 0$, $n_2 = \frac{2}{3}n$ and $n_1 = 0$. In the context of the model, this works perfectly. There is no way to create n_1 without helium. Then in both cases, as helium density increases, the density in each excited state grows until the two states have near the same density, $n_1 \approx n_2 \approx {}_{\bar{2}}5n$

Similar analysis needs to be done for the two doubly excited states as well. For the density in the 5^2D doublet, n_3:

$$\frac{dn_3}{dt} = k_{p3}(n_1 + n_2)^2 - k_{q3}mn_3 - \xi_3 A_3 n_3 = 0 \tag{15}$$

$$n_3 = \frac{k_{p3}(1 - \frac{1}{2\gamma-3})^2}{k_{q3}m + \xi_3 A_3} n^2 \tag{16}$$

The values for n_1 and n_2 were taken from Eqs. 13 and 14. A quick analysis of these equations show that n_3, as a function of helium density, may initially rise, as γ's intial increase will drive the function up. This may not last long, though, as the m dependence in the denominator will become dominant and begin to pull the density back down. The magnitude of the initial increase though is dependent on the value of the quenching rate.

The last density is that in the 6^2D doublet, n_4, and its rate equation is:

$$\frac{dn_4}{dt} = k_{q3}n_3 m + k_{p4}(n_1 + n_2)^2 - (\xi_4 A_4 + k_{q4}m)n_4 = 0 \tag{17}$$

$$n_4 = (\frac{k_{q3}k_{p3}m}{(k_{q3}m + \xi_3 A_3)(k_{q4}m + \xi_4 A_4)} + \frac{k_{p4}}{k_{q4}m + \xi_4 A_4})(1 - \frac{1}{2\gamma + 3})^2 n^2 \tag{18}$$

It is much more difficult to understand helium's dependence on this state simply by inspection. To simplify this, the term consisting of k_{p4} might be neglected. The process of energy pooling to the 5^2D state is a much faster process than the pooling to the 6^2P state, so $k_{p3} >> k_{p4}$. In spectroscopy it is known that the transition $5^2P \rightarrow 6^2P$ is not an electric dipole allowed transition. This is because the matrix element associated with the electric dipole operator is 0. If the operator that dictates the energy pooling process looks like the dipole operator –i.e. goes like $\hat{r}$– then it too will not be an energy pooling allowed transition. Furthermore, energy pooling rates have been calculated in cesium and it has been shown that k_{p3} is nearly two orders

of magnitude greater than k_{p4} (12).

With this simplification, the behavior of the density in the 6^2P states as a function of helium is a bit simpler. The same γ factor is in this equation as in 16, so you would again expect an initial increase of density. However, unlike in 16, there is an m in the numerator as well. It has the functional form $\frac{x}{(x+1)^2}$, which has an initial rise until the $(x+1)^2$ in the denominator overtakes the x in the numerator. So it seems that the density in 6^2P will demonstrate a much larger rise and continue rising for longer, before it turns and begins to decrease as the helium pressure grows.

The final model is present below. Due to scattered pump light, it is impossible to compare the density of n_2 to the data. However, the other states can easily be compared to spectroscopic data, and they are in a future chapter.

$$n_1 = \frac{1}{1+\frac{3}{2}\frac{1}{\gamma}}n$$

$$n_2 = \frac{1}{\frac{3}{2}+\gamma}n$$

$$n_3 = \frac{k_{p3}(1-\frac{1}{2\gamma-3})^2}{k_{q3}m+\xi_3 A_3}n^2$$

$$n_4 = (\frac{k_{q3}k_{p3}m}{(k_{q4}m+\xi_3 A_3)(k_{q4}m+\xi_4 A_4)} + \frac{k_{p4}}{k_{q4}m+\xi_4 A_4})(1-\frac{1}{2\gamma+3})^2 n^2$$

III. Experimental Apparatus

Flouresence of rubidium vapor excited along the D_2 transition by a pulsed dye laser is examined to obtain relative concentration of different energy levels. The experimentation was done in a custom Pyrex cell. The Pyrex cell was heated to temperatures between 195°C and 235°C. The rubidium was heated in a custom aluminium heater block, with a Watlow DUAL-ARGR-1300 controller using 10 Watlow C1J6-L12H heater plugs, monitored by a K-type thermocouple. The rubidium density in the cell at these temperatures was then found using vapor pressure curves (2). At these temperatures, the rubidium denisty in the cell is $n = 10^{14} - 10^{15} \frac{1}{cm^3}$. The rubidium itself came from Alfa Aesar and has a 99.75% purity, with caesium as the leading contaminant. The pump laser consisted of a Coninuum Surelite 3 ND:Yag doubled to 532nm pumping a Continuum ND 6000 tunable dye laser with Exiton LDS 765 dye. The pump laser had an average output power of around 25 mJ per pulse with a nearly circular spot size with a radius of approximately 0.3 cm. The laser had a rep rate of 10 Hz and a pulse that last around 10ns. This corresponds to intensity of 8.85 $\frac{MW}{cm^2}$. Helium was injected through an arm on the top of the cell, coming through a system of Swagelok and Ultra-Torr fittings. The maximum helium pressure the cell could withstand is near 1200 torr; pressure was kept below 1000 torr as to not exceed the limits of the Ultratorr fitting. An MKS Type 670 Signal Conditioner was used to monitor Helium pressure in the cell. The Helium was 99.999% pure from Weiler Welding Company. The system had a total leak rate of ¡.002 Torr/sec.

The florescence was captured using an Acton SpectraPro 275 spectrometer with a Princeton Instruments, PI-MAX 2 CCD camera attached, being viewed from the side as shown in Fig. 3. Initial attempts were made to view the cell transversely but the scattered pump intensity made it impossible to capture any of the other, less intense lines. The detector had a spectral resolution of 0.031 nm over the range of 275-925 nm.

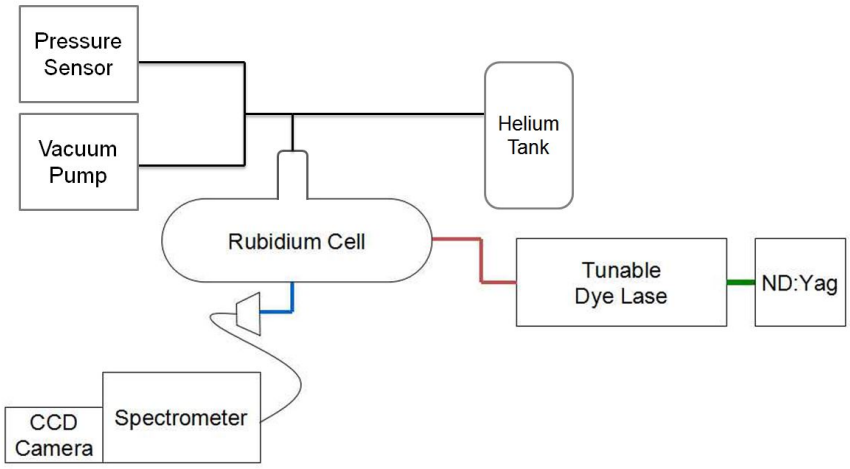

Figure 3. Block Diagram of the apparatus used in this experiment. The florescence was viewed from the side made capture of many transitions possible. Space limitations caused the seemingly unnecessary florescence reflection

Exposure time of the spectrometer was between 200-400 ms, and was only modulated in 100 ms increments. This ensured that multiple pulses were captured. Futhermore, if it is assumed that the pulses are equally spaced, by increasing exposure time in steps of 100 ms, it can be assured that an equal number of pulses are captured in each exposure. AS long as the exposure time is constant over a given data collection, there is no possibility of capturing different numbers of pulses. The PI-MAX Camera has an aperture approximately 30 nm across, scans were taken every 25 nm, starting at a center wavelength of 300 nm to a center wavelength of 900 nm, covering the effective range of the spectrometer. The Acton spectrometer had two gratings, each with 1200 grooves/mm, one with a blaze wavelength of 300 nm and the other with a blaze wavelength of 750 nm. The grating switch took place at a center wavelength of 575 nm and was carried out for every run-through to keep consistency between runs. The background noise was near 500 counts and all signals required a peak above 2 times the noise to be recorded. The system was calibrated for intensity first using a quartz halogen lamp and then a black body emitter, for a more in depth analysis on the calibration see Appendix A.

IV. Results

4.1 Ionization

A sample spectra is shown in Fig. 4 and Fig. 5. The largest peak is at 780 nm, the D_2 transition. Some of its intensity though comes from the scattering of the pump beam. The figured has been zoomed, and the D_2 and D_1 transition's peak magnitudes have been clipped to show more details of the smaller peaks. The D_2's true peak height is approximately $5 * 10^1 1$ photons and the other has a magnitude near $2 * 10^1 1$. The next highest peak occurs near 795 nm, this is the D_1 transition. These two peaks make up the entire DPAL process. The only other peaks that are expected from the model are the ones at 420 nm, 421 nm, 761 nm, and 775 nm. The peak intensities of the lines are calculated as an estimate of the area under the peak.

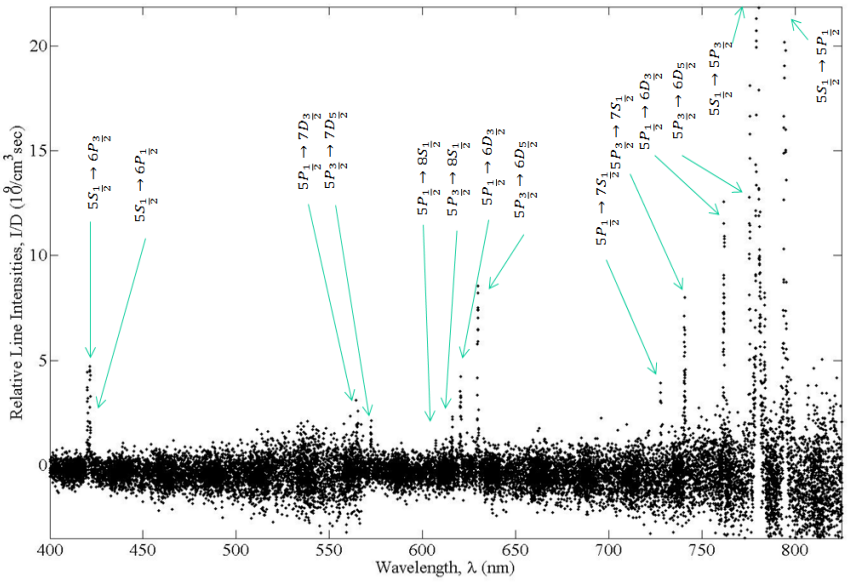

Figure 4. Sample Spectra of the rubidium laser induced flourescence. This spectra was recorded with no added helium and a cell temperature of $225°C$. This spectra has already taken into account detector response, the units on the y-axis are relative spectral intensities.

The numerous other peaks present indicate a phenomenon not yet accounted for

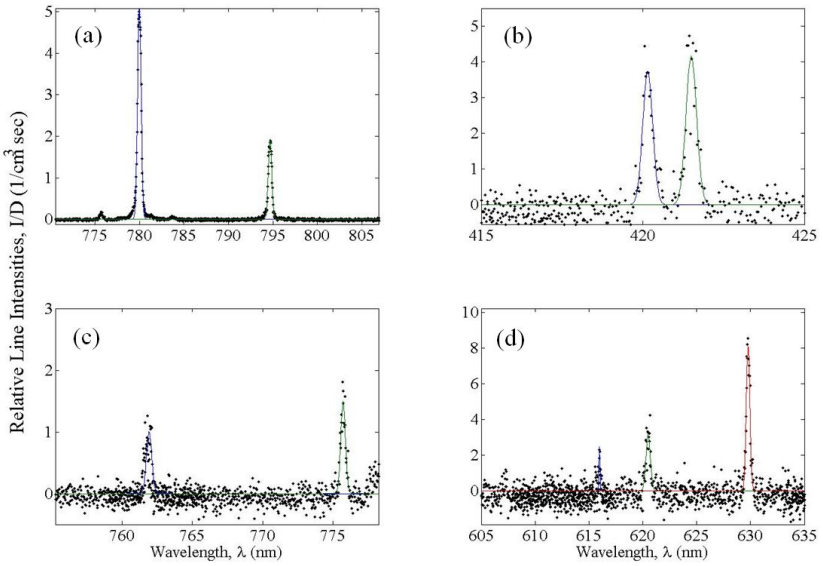

Figure 5. Zoomed in veiw of some of the spectral lines above. (a) The D_1 and D_2 transmission lines, in 10^{11} counts. Some fraction of the 780 nm line may be scattered pump laser though. (b) These lines stem from the 6^2P states, in 10^9 counts, and represent n_4. (c) The population n_3 can be derived from these two red lines and have the 5^2D state the initial state, here in 10^{10} counts. (d) Some of the minor transitions observed, in 10^{10} count. Their intensity falls away quickly as buffer gas is added.

in the presented model. They were neglected in the model because their intensities are theoretically much smaller than those of the major transitions. These minor transitions probably suggest that ionization is in fact occurring. The recombination of the rubidium ion with a free electron is the primary mechanism for creating these highly excited states. Most of the minor transitions are either $D \rightarrow P$ and $P \leftrightarrow S$ (26). While population in higher S states can be created by collisional energy transfer (22), it is much more likely that electron recombination is the source for this excited population. In Fig. 6 the helium dependency of the minor transitions, at $235°C$, is shown. At its most intense, the densities in all of these minor energy states is only 10% of the population in the lower lying states. Relative concentration of the 6^2P and 5^2D states have a nonzero asymptote; however the population in the higher excited states falls to zero before 400 torr of helium. This seems to suggest that in pulsed experiments the effects of ionization are negligible for higher buffer gas pressures.

The DPAL is often run with buffer gas pressures above 400 torr (16), so this evidence shows that ionization may not be an issue for pulsed DPALs.

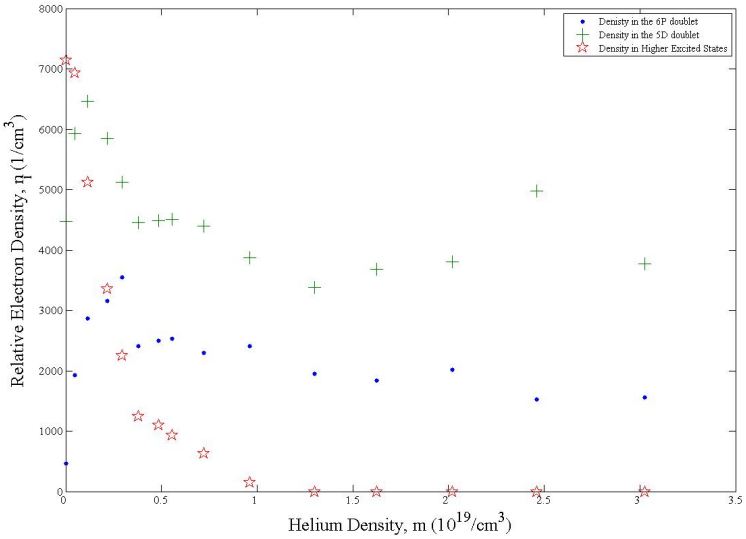

Figure 6. The densities of the highest excited states vs helium density. The density in the highest exctied states, all of those higher than the 5D doublet, disappears into the noise fairly soon. The other two states reach an asymptotic limit greater than zero. The implication is ionization seems to fall away completely at higher buffer gas pressures.

Additionally, no spectral lines were observed from the rubidium ion. There exist hundreds of lines in the visible spectrum from electron transitions for Rb^+ but none were observed. It is true that the first excited state in the rubidium ion may be difficult to reach, with an energy over 130,000 cm^{-1}, compared to the approximately 13,000 cm^{-1} of the lowest level of the rubidium atom (14). However, if the degree of ionization was high enough, free electrons could accrue enough energy to populate these extreme states. Their absence may be additional evidence that ionization is not a major mechanism in this process. Spectral lines from the rubidium ion were observed when pumping along the two photon process decribed in (24). The $5^2S_{\frac{1}{2}} \rightarrow 5^2D_{\frac{3}{2}}$ transition, for instance, is identified at 424.4 nm. This seems to implicate that the ionizational effect is much greater in that experiment.

Fig. 7 shows the decrease of highly excited rubidium density at different cell temperatures, and therefore total rubidium density. This clearly shows that the buffer gas pressure needed to completely quench these transitions is directly proportional to the total rubidium density. An optimized power-scaled DPAL has been shown to require cell temperatures of under $140°C$ (6). This too implies ionization may not be an issue in real DPAL applications.

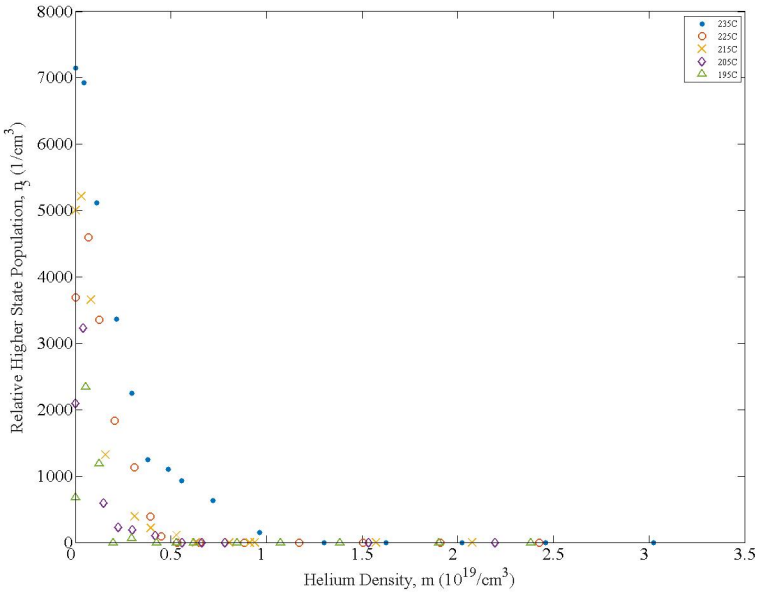

Figure 7. The densities of the highest excited states vs Helium density at different temperatures. The • represents taken collect at a cell temp of $235°C$. The ∘ is at $225°C$, × is $215°C$, ◇ is for $205°C$, and the △ is for $195°C$. As the total Rubidium density increases, the Helium pressure necessary to quench all of the tranistions from the highest energy levels increases as well.

4.2 Model Analysis

The model constructed in Chapter II was fit to the experimental data collected. The first step to fitting the model was to find a functional form for the trapping factor. With the only condition on the functional form of the trapping factor being that it is a decreasing function bounded above by 1 and below by 0, there were many

possible options that fit. A simple form that fit well, with only two parameters, was $\xi \propto \frac{1}{(1+bn)^k}$. This allowed for greater control of the rate of decay. To experimentally determine the values for b and k, the intensity of the D_1 line was monitored as a function of rubidium density, at a high value of buffer gas. From the model, it can be seen that, given $M >> 1$, then the density in the $5^2P_{\frac{1}{2}}$ goes like $n_1 = \frac{2}{5}n$. Using this and the experimental data,

$$\frac{I_1}{A_1 \mathcal{D}_1} = \mathcal{D}_a \xi_1 \frac{2}{5} n \tag{19}$$

where I_1 is the intensity of the D_1 line, $\mathcal{D}_1$ the relative detector response at 795 nm, and $\mathcal{D}_a$ is the absolute detector response. The relative detector response is the fraction of a known photon input that registers a count on the detector and is different for every wavelength. On the other hand, the absolute detector response is a function of the geometric set up and relates the number of photons theoretically emitted to the number of photons that reach the detector. Fig. 8 shows the fitting of Eq. 19 to the D_1 line intensities, as a function of total rubidium density, at 549.9 Torr of helium. The decrease of apparent population demonstrates the effect of radiation trapping. Even though the $5^2P_{\frac{1}{2}}$ is increasing, the increase in total population is causing a decrease in the rate of photon escape. The general shape of the curve gives the form of radiation trapping, and the amplitude sets the value for the absolute detectivity of this set-up.

Now that the parameters in the model are set, an attempt to match the helium dependence of D_1 with the data is attempted. The dots in Fig. 9 represent the data. The blue dashed line represents Eq. 14 with the parameters as were just derived. It seems that the model is not a very good fit. However, corrections can be made to better predict the data, and the red and green lines represent the model as these improvements are made. The first major flaw is the general shape of the fitted line, it

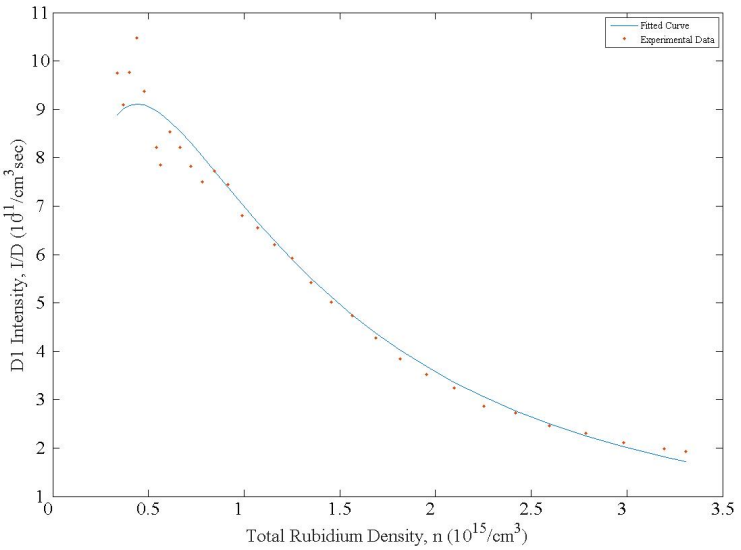

Figure 8. The intensity of the D_1 transition as a function of Rubidium Density. The expected rise in D_1 intensity due to the increase in Rubidium is subverted due to the density dependence in the trapping. The fit equation looks like $I = \frac{.0067}{(1+9*10^{-16}n)^{3.52}}$.

approaches its asymptotic limit much too quickly. This inaccuracy can be attributed to an apparent decrease of the total rubidium density. This error comes from two different sources. First of all, the initial values used for the total rubidium density are taken from the vapor pressure curve from (2). This assumes the cell is heated uniformly to the temperature registered by the thermocouple. In truth, the average temperature is some number slightly less than that, so it serves a upper bound.

The more important issue, though, is what will be referred to as the diffusivity problem. The solid rubidium is kept in a small off-chute of the cell below the main chamber, where the pump laser goes through. When helium is added from the top of the cell, its much greater pressure forces the gaseous rubidium down into this bottom finger. It then takes a significant amount of time for the rubidium to work its way back into the main cell. In this time the true rubidium density actually in the pump's path is significantly depleted. Fig. 10 shows that it takes nearly 45 minutes for the rubidium density in the cell to equilibrate, and any data taken before that time will

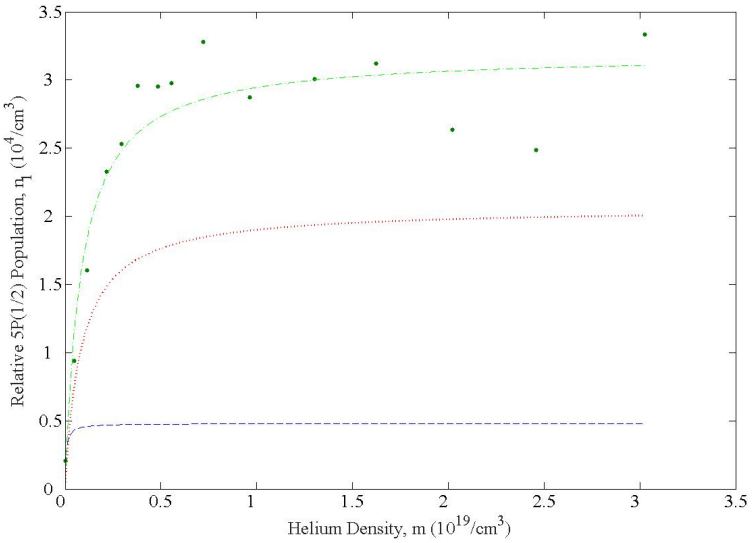

Figure 9. The intensity of the D_1 transition as a function of Helium Density. The blue lines represents the initial prediction of the model. The red line shows the prediction becoming marginally better when diffusivity is corrected for. The model predicts the data very well when the laser degradation is fixed, shown here in green.

suffer from a much lower density. Unfortunately, this diffusivity issue was identified well after the main data was taken and the data was captured before the cell was able to come back to equilibrium. This diffusivity issue can be expressed in the model by changing the true density to some much smaller value, n_{app}. This modification allows us to slightly change the shape to correct the growth rate. It was found that $n_{app} \approx .2778 n_{true}$. That is not to say that it is believed that the rubidium densities presented in Fig. 8 are absolutely correct, but due to experimental methods, they are believed to be much closer to the true values. This change of the model moved the prediction to the red dotted line in Fig. 9.

This first correction has not completely solved the problem, though, as the magnitude is still incorrect. The primary reason for this can be attributed to a degradation in laser power. One of the initial assumptions made was that there was no radial dependence on the fluorescence inside the cell. If this were true, then once the rubidium is bleached all the way through the cell, adding more pump power would not cause

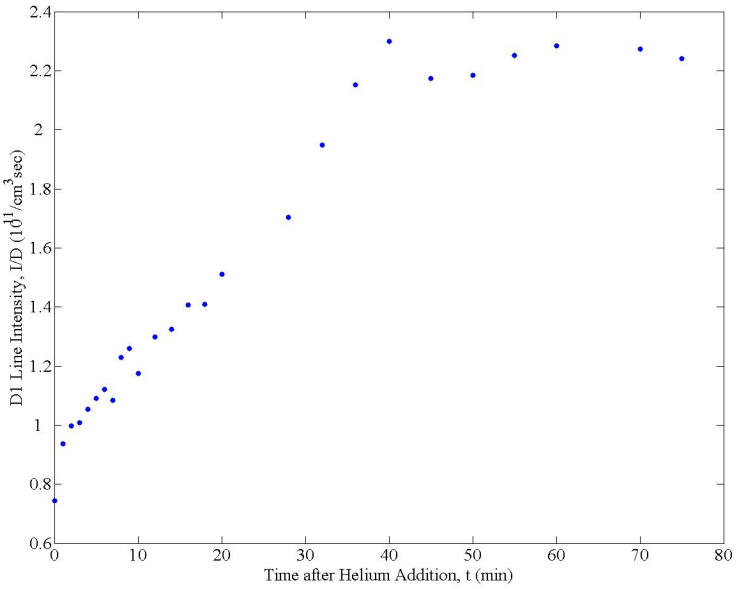

Figure 10. The intensity of the D_1 transition as a function of time after buffer gas addition. It appears that it takes nearly 45 minutes for the gas in the cell to reach a stable density. Data taken before that time will be subject to inaccurate density measurements.

additional rise in transition intensity. This, however, is seen to be not true. Even though the rubidium is bleached the entire length of the cell–the pump intensity is 10^6 times that of the saturation intensity, the intensity of the D_1 transition grows with pump laser power, as seen in Fig. 11. Fig. 11 also shows that the intensity for the other transitions also grows, and it grows with a similar rate as the D_1 transition. The fact that all three transitions grow linearly implies that this may be due to the to an increase in the radius of bleached rubidium in the pump beam. If it were true that the cell was not bleached all the way along its transverse axis, then this increase in laser power would create a linear rise in the D_1 line, but the other transitions should have a different shape. Eq. 16 shows that the 760 nm line would grow quadratically compared to the D_1 transition. This phenomenon was discussed in Chapter II.

The data shown in Fig. 8 and 9 was taken nearly a month apart. In this time, the laser dye being used to tune the pump laser began to become exhausted. The

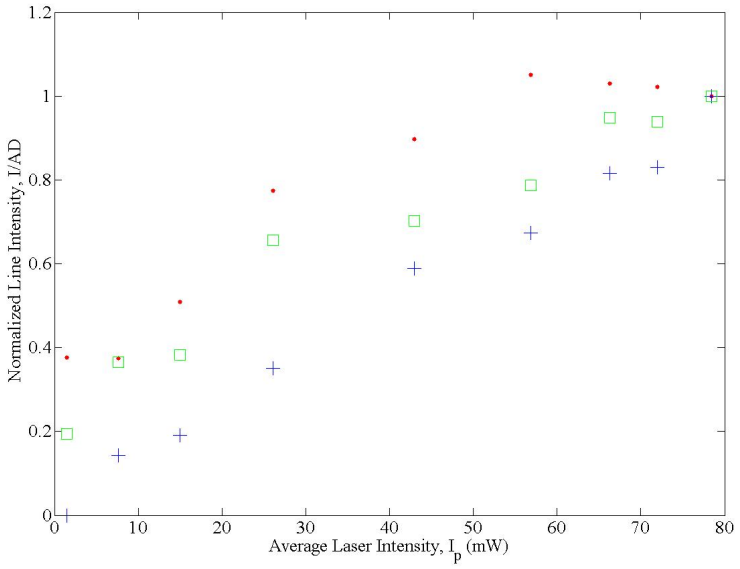

Figure 11. The pump beam intensity vs. the normalized transition intensity. The dots represent the 795 nm line, the plus signs are for the 420 nm line, and the squares represent the 761 nm transition. All the monitored transitions' intensity rises linearly with respect to pump power. This can only be caused by an increase of the radius of the bleached volume.

effectiveness of the dye reduces over its working lifetime and pump intensity was nearly halved in that time, from approximately 35 mJ per pulse of pump intensity to under 20 mJ. While the rubidium was still bleached at the lower pump power, the decrease in bleached area could cause the amplitude discrepancy that is being seen. The amplitude of the predicted line is adjusted to a higher value account for this degradation. The final correction is shown as the green dashed/dotted line in Fig. 9.

A similar process is undertaken to fit the model to data of the 761 line. The functional form of the trapping for this transition has a simliar functional form as was selected before. It is given as $\xi_3 = (1 + bn)^{-3.52}$. It is posited that the value of the exponent must be constant over all transitions, as the form of trapping should be the same, but the value of the parameter b can be variant between transitions, as it encompasses the absorption cross section and that will change for each transition. From Eq. 16, at large values of buffer gas, the intensity of the 761 nm transition goes

as:

$$\frac{I_{761}}{\mathcal{D}_3 A_{761}} = .267 * \mathcal{D}_a (1+bn)^{-3.52} n^2 \frac{k_{p3}(\frac{4}{5})^2}{k_{q3}m + A_3(1+bn)^{-3.52}} \tag{20}$$

An important distinction must be made between A_{761} and A_3. A_{761} is an estimated A-coefficient for the transition $5^2D_{\frac{3}{2}} \rightarrow 5^2P_{\frac{1}{2}}$ whose responsible for the 761nm line. A_3 is the sum of all A-coefficients with $5D$ manifold as the upper state. It comes from the total radiative lifetime of the state, found experimentally in (25). The value of pooling cross section of this energy level is taken from (27) and the rate constant is found to be $k_{p3} = 5.9199 * 10^{-10} cm^3 sec^{-1}$. The constant in front of $\mathcal{D}_a$ is an approximation of how much of n_3 would emit along the 761 nm transition. It takes into account the degeneracies of the 5^2D manifold, as well as the proportion of photons emitted along at this wavelength, as opposed to those along the $5^2D_{\frac{3}{2}} \rightarrow 5^2P_{\frac{3}{2}}$ transition.

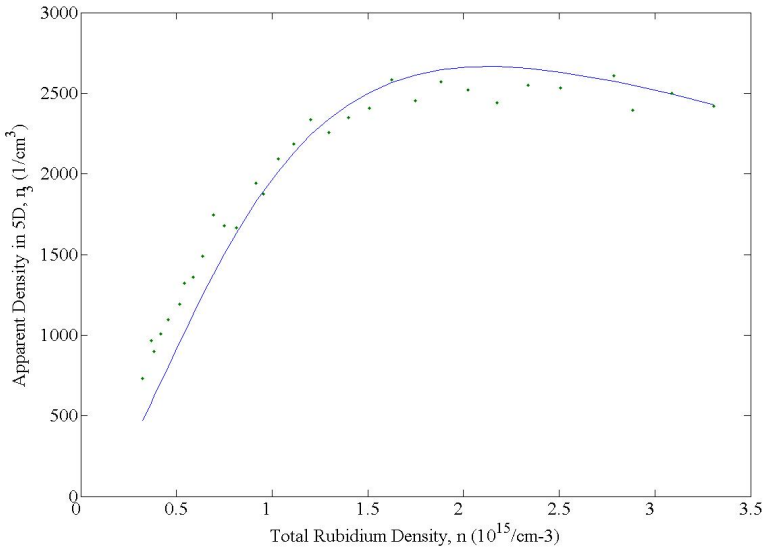

Figure 12. Apparent density in the 5D states as a function of rubidium. The helium pressure was held constant at approximately 700 Torr. Eq. 20 is fit in the high helium denisty limit and the functional form of the trapping factor is set with this plot. The trapping constant, b, is changed though to account for absorbance differences.

Eq. 20 is fit to the experimental data in Fig. 12. The trapping seems to be much less for this transition though it still rises initially as total density is increased.

The reduced trapping of this transition is to be expected, as the population of atoms that could reabsorb this photon (ones in the $5^2P_{\frac{1}{2}}$) is much less than those in the ground state. It is true that in the pump laser path, the population in the $5^2P_{\frac{1}{2}}$ is higher than that in the ground state, in the rest of the volume of the cell the excited population is much lower than that in the ground state. The functional form of the trapping factor fits this data as well, so it verifies the functional form chosen. The only value left to determine from Eq. 16 was k_{q3}. Eq. 16 is fit to experimental data in Fig. 13. The model does a very poor job of correctly predicting the data, the asymptotic limit is close but the amplitudes near 0 buffer gas is much too high. The shape though has similar features, the prediction initially rises with helium before quickly falling, just like the data. The estimated value for the quenching of this state is $k_{q3} = 1.34 \pm .9 * 10^{-13} cm^3/sec$

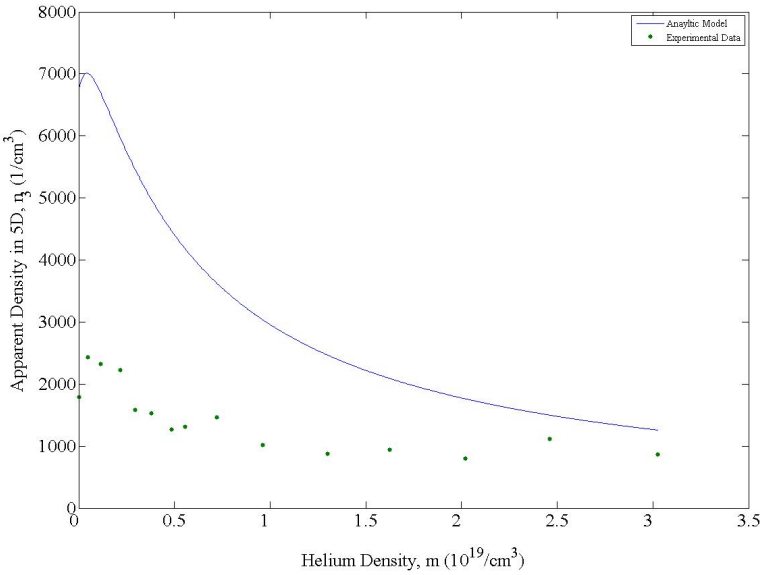

Figure 13. Density in the 5D states as a function of Helium. The model created in Ch. II is compared to the actual data. Many mechanisms were neglected in the creation of the model and it seems like at least one addition is required.

It may be that either diffusivity or laser degradation is causing this inconsistency, but it seems like there is a much bigger issue at play here. Before possible modifica-

tions to the model are introduced, the final fitting of the data should be completed. Keeping the same functional form for the trapping, the model is first fit when $M >> 1$ to find an estimate for the quenching rate for these excited states. For this state we want to look at the entire manifold:

$$\frac{I_{420}}{\mathcal{D}_{420}A_{420}} + \frac{I_{421}}{\mathcal{D}_{421}A_{421}} = \mathcal{D}_a(1+b_4 n)^{-3.52} n^2 (\frac{4}{5})^2 \frac{k_{p3}}{k_{q4} m} \tag{21}$$

Again, it is allowed for the value of the parameter b_4 in the trapping to be different from that of the other transitions due to differences in absorbance. It will be required though that the trapping for both of these transitions to be the same, as their wavelengths are so similar. The A-coefficients used here are transition specific, and a difference must be noted between those and A_4 which will come up shortly and is $A_4 = A_{420} + A_{421}$. Eq. 21 is fit to experimental data with a helium pressure of 549.9 Torr and a value for k_{q4} is determined, in Fig. 14. The trapping seems to be at a rate in between the two previous transitions.

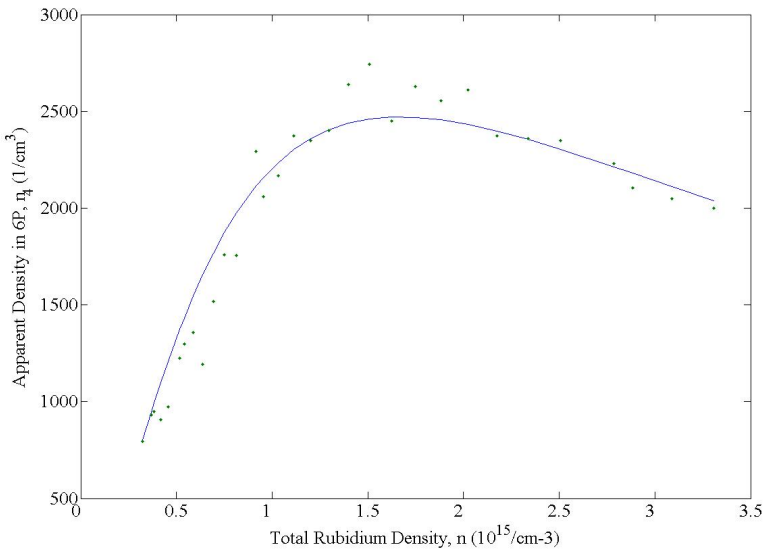

Figure 14. Apparent density in the 6P states as a function of Rubidium. The same functional form of trapping is utilized, again with slightly a different b parameter.

Using these fit parameters with Eq. 18, the model is completed, in Fig. 15. The same issue is seen in the $6P$ manifold as in the $5D$. The model's magnitude is much to high, expecially at low buffer gas densities. The evidence points to a major mechanism being left out of the model. Recall, the model presented is one possibility. Possible corrections to this model can found below.

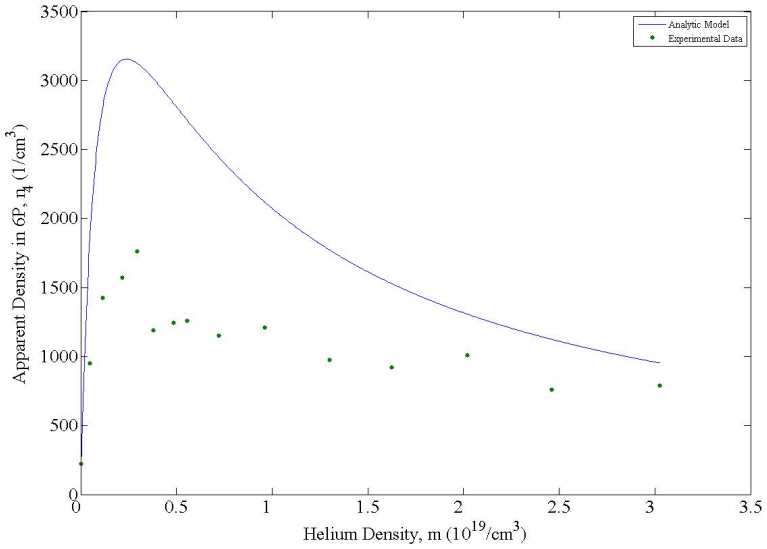

Figure 15. Density in the $6P$ states as a function of Helium. The model created in Ch. II is compared to the actual data. This has the same over estimation of density that is seen in the $5D$ model, and requires additional mechanisms in the model.

4.3 Model Corrections

While this model fits the experimental data relatively well for the D_1 transition, there still exists some major disparities in the other transitions. The denisty predicted is much to high at low helium densities, as seen in Fig. 13 and 16. The size of this incongruity implies that the model itself is missing something. And, due to the closer agreement of the graph at high helium densities, it can be assumed that this missing mechanism is not a function of buffer gas density. The first thought is ionization. As shown in section 4.1, at low helium pressures, ionization is an important mechanism

in the physics in the photoluminescence. And yet it is not incorporated into the model in any way. This seemingly would work to as a correction. It would only affect the higher excited states, so the model of the D_1 transition would be unchanged, but the others would have a new term in the denominator of each of its densities. Furthermore, at high helium densities, any term that is a function of helium would dominate and lessen the effects of ionization, bringing the density down more when helium is small.

A simple process of photoionization can be added to the model. This mechanism can be written as:

$$N_{3,4} + h\nu \overset{k_{I3,I4}}{\rightarrow} Rb^+ + e^- \tag{22}$$

Here $k_{I3,I4}$ are the ionizaiton rate of the 5^2D and 6^2P manifolds, given by $k_{Ii} = \frac{\sigma I i I_P}{h\nu}$ where σIi is the ionization cross section of the excited states, I_p is the pump intensity and$h\nu$ is the energy in a pump photon. The equation for the $5^2P_{1/2}$ remains unchanged when ionizaiton is added, however the other two look a bit different:

$$n_3 = \frac{k_{p3}(1 - \frac{1}{2\gamma+3})^2}{k_{q4}m + k_{I3} + \xi_3 A_3} n^2 \tag{23}$$

$$n_4 = (\frac{k_{q3}k_{p3}m}{(k_{q3}m + k_{I3} + \xi_3 A_3)(k_{q4}m + k_{I4} + \xi_4 A_4)} + \frac{k_{p4}}{k_{q4}m + + k_{I4} + \xi_4 A_4})(1 - \frac{1}{2\gamma + 3})^2 n^2 \tag{24}$$

Fig 16 demonstrates the power of this additional mechanism. The blue solid line is the same fit from Fig. 13. The red dashed line a fit with ionization added. This perturbation lowers the modelled density by nearly half in the low buffer gas region, while staying close in the high buffer limit. The quoted value for the ionization cross section of the 6^2P manifold in rubidium excited by a 694 nm pump laser is around

$1.5*10^{-17}cm^2$ (3). Fitting the data with a 795 nm pump laser sets the ionization cross section of the 5^2D manifold to $7.2*10^{-}18cm^2$. There is obviously still a piece missing form this picture, as the model still over predicts the data. While it seems that ionization does make the model better, there are still issues. The possible problems, both experimental and analytic, will be discussed in the following chapter.

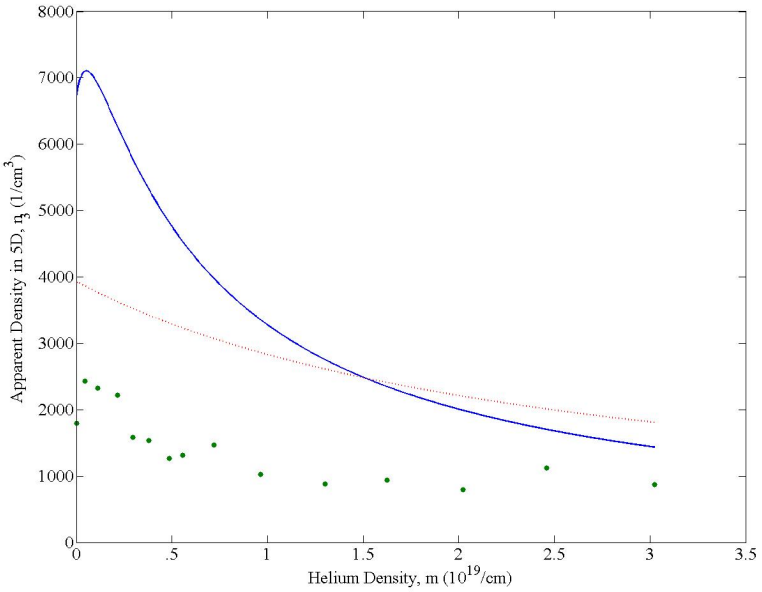

Figure 16. Addition of ionization to the presented model. The solid line represents the original model adn the dashed line represents the model with the ionization correction. It seems like this improves the model but does not entirely correct it. This implies that an additional mechanism is necessary.

Another possible mechanism that would lower the density of the highly excited states is self-quenching. In the same way that collisions with buffer gas can cause a relaxation to lower energy, so to would collisions with itself. As you increase helium density the relative magnitude of this self quenching term compared to the buffer gas quenching would become negligible, but near vacuum, it could be a way to deplete this doubly excited density. It could also be that these energy states are transitioning to other states in transitions that cannot be captured with this setup. There exists transitions whose photons have wavelengths outside the visible and it could be in

those transitions that these states are becoming depleted. The 5^2D to 6^2P transition would occur at approximately 5 μm. These longer transitions could account for the incosistencies in the model and serve as a mechanism other than ionization that could correct the model. The following chapter will suggest ways to better the model and suggest experiments that may provide evidence for each mechanism.

V. Future Work and Conclusion

Emissions from the higher lying states of atomic rubidium after pulsed excitation of the $5^2P_{\frac{3}{2}}$ state in the presence of helium has been used to study energy pooling an ionization. For rubidium densities below $n = 2.06 * 10^{14} cm^{-3}$ emission is limited to the D_1 and D_2 lines arising from the $5^2P_{\frac{3}{2}}$ and the collisionally populated $5^2P_{\frac{1}{2}}$ states. At higher alkali density populations $n < 3.31 * 10^{15} cm^{-3}$, emission from 13 lines have been observed for peak pump intensities of $1.5 MW/cm^2$.

Population in the 5^2D and 6^2P appears to arise from energy pooling and persists for helium pressures as high as 940 Torr. At higher alkali densities and strongly bleached conditions, the emissions from all of the major energy states is strongly trapped. The spontaneous emission rates from the 5^2D and 6^2P manifolds are reduced by around 10, and the same rate of the D_1 transition is reduced by a factor of nearly 100.

Population in the states above 5^2D decrease significantly with added helium and are fully quenched at 500 Torr, much lower than the buffer gas pressures needed to efficiently operate a DPAL. The dependence of helium pressure on emmision intensity is complicated by a very slow diffusion rate ($\approx$ 1 hour). These highly excited states are likely produced by ion recombination.

No emission from ionic rubidiumhas been observed even at pump intensities of $1.5 MW/cm^2$ The first exctied stated of the rubidium ion, Rb^+, is at 16.53 eV above the ground ion state (14), requireing high electron kinetic energy which appears to not be achieved when pumping the D_2 transition. However, an emission line from the rubidium ion's $5P$ state can be observed when pumping the two photon $5^2S_{\frac{1}{2}} \rightarrow 5^2D_{\frac{3}{2}}$ transition.

Efficient DPAL operation with surrogate pulsed pump lasers have been demonstrated at pump intensities exceeding $10 MW/cm^2$, several orders of magnitude greater

than achievable with current diode laser technology. Three pump photons are required to reach ionization. The DPAL system depends on the first photon exciting to the $5^2P_{\frac{3}{2}}$ state. The mechanism for excitation to a higher excited intermediate state is unclear but slow. Once in a highly excited state another pump photon can readily ionize the alkali. The slow step to produce the higher excited intermediate appears to limit ionproduction during the short pulse duration of the current experiments.

Several additional experimetns are required to continue this study and explain the effects of ionization on DPAL performance. First, this data should be recollected taking into consideration diffusivity and laser power degradation. Issues with the radial dependency in the photoluminecence can be sovled by careful observation of the pump laser power or implementation of pinhole to limit the field of view should clear up some of the issues; although too much blocked intensity could result in a drastic decrease in received signal.

Waiting for the cell to equilibrate after the injection of helium is the obvious solution for the diffusivity problem. Additionally, it would be possible to experimentally monitor the rubidium density in the cell immeadiately before data collection. Using the absorption spectrum of a broadband light source along prominent transition lines, the total rubidium density can be derived. These issues could call into question the validity of the quantitative results presented here. Moreover, this investigation may result in a roll off of intensity in the D_1 transition at higher pressures; it must be certain that this roll off is not due to fluctuations in the apparent number density.

These mistakes in experimental methodology are not the only unresolved issues. Radiation trapping is a much bigger issue. The functional form chosen seems to work, but it is surely not the only function that could fit. The biggest cause for error in this could be the amplitude of this trapping. The trapping factor used in this analysis is seemingly independent of buffer gas pressure. Intuitively, this does not

make sense, as the broadening of line shape should have some effect on the radiation trapping observed. To get a more accurate functional form for trapping, collection of line intensity as cell temperature is increased at many different pressures should be undertaken. With multiple graphs like Fig. 8, a more complete picture of the trapping can be created. A more rigorous anayltic solution may be instead obtained to fit to the data. The Holstein equation governs the trapping mechanism (18), and has eigenvalue solutions that go like the sums of exponentials. A more correct functional form for the trapping observed will allow for a more accurate description.

Another useful piece missing from this study is the D_2 transition intensity. Theoretically, it can be used as a comparison tool to find absolute densities for these upper states. The absolute density of this state can be easily derived using the total rubidium density, assuming the transition is bleached, and its ratio with the other transitions could produce absolute densities for those states as well. Furthermore, this ratio will strip away some of the uncertainty due to diffusivity and laser degradation. Data was collected for this D_2 transition, in Fig. 4 for instance, but radiation trapping makes it useless at this point. Some of this intensity is coming from scattered light from the pump beam, but there should be some being re-emitted by the rubidium. The trapping makes it impossible to decouple the scattered pump intensity from that being emitted from electron relaxing to the ground state. Fig. 17 shows the comparison of the pump laser on and off resonance. The pump intensity of the laser on resonance is much less than the pump intensity off resonance. Radiation trapping causes this severe decrease. It is unknown the degree to which the trapping is suppressing the intensity, but there is no reasonable upper bound to this inflation.

The experimental set up used also caused limitations in the experiments completed. The glass cell made it dangerous to heat the cell much past $235°C$ and impossible to inject more than around 1.5 atm of helium. It seems that with higher

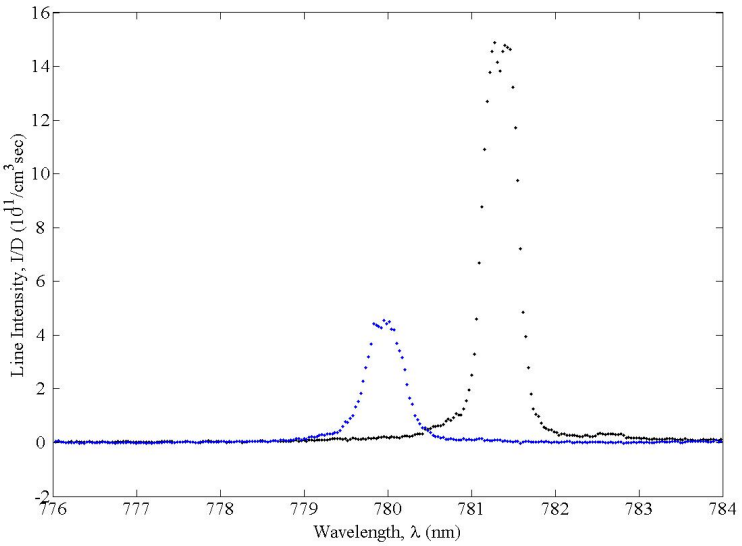

Figure 17. Effect of trapping on scattered pump beam. This large increase when moving off resonance indicates that trapping plays a huge role. But because the degree of trapping is unknown, it is very difficult to decouple the two phenomenon.

cell temperature, and rubdium density, the minor transitions are much more intense and it would be possible to characterize their behaviors with a model similar to the ones presented previously. It is also important to ramp up the helium pressure. Existing pure helium DPAL systems require helium pressures of 4 atms to run (31), and the more rubidium in the cell, the more helium required to maximize the D_1 output. It is essential that those high density and pressures are investigated.

It also would be wise to explore transitions that fluoresce outside the visible spectrum. Photons with longer wavelengths have been observed in rubidium–lasing between between the 5^2D and 6^2P has a wavelength around 5 microns, for instance (14). The intensity of these lines may provide more insight to the mechanisms surrounding ionization and recombination. These include tranistions in the Near IR and IR and some that would come from transitions in the rubidium ion. This experiment was limited by the detector system used, it was only able to capture photons with wavelengths under 900 nm. A new spectrometer and camera system would allow for

the observation of these new transitions.

The last experiment that will be discussed is the change from a pulsed pump laser to CW one. It has been shown that the roll off of output power occurs much sooner when using a continuous pump beam (5). The time between pulses may be all that is needed to relax enough rubidium from excited states to cause a substantial decrease in the effects of ionization. If the 5^2P manifold is continuously bleached, it may cause an increase in the energy pooling that seems to cause the ionization to the point of significantly hurting the output intensity of the D_1 transition.

With the data collected thus far, few definite answers can be made. It is certain that the model presented needs an additional piece to fix the over estimation of the data. It is also certain that at low buffer gas pressures, highly excited states are becoming populated, and it could be that photoionization is responsible for its creation. But the concentration in these states fall to 0 when the moderate amounts of buffer gas is added. Radiation trapping plays a major role that requires much more investigation. With a more accurate description of trapping effect, a more accurate model can be created and an ionization rate could be derived for both pulsed and CW DPAL systems, ultimately settling this heated debate.

Appendix A. Calibration

Callibration of the Acton Spectrometer was completed using both a broad spectrum quartz halogen lamp, Oriel Instruments model number 5-123, and a blackbody emitter, Electo-Oprical Industries LS1350-100. For the halogen lamp, a spectral irradiance is quoted by the manufacturer for a distance of 50 cm from the lamp. The equation is given as:

$$I = \lambda^{-5} * e^{42.98953 - \frac{4583.98173}{\lambda} + \frac{211819}{\lambda^2} - \frac{1.4232551E8}{\lambda^3} + \frac{3.847842E10}{\lambda^4} - \frac{3.8965903E12}{\lambda^5}},$$

where I is irradiance in W/m^2nm, λ is the wavelength in nm, h is Plank's constant, and c is the speed of light. Taking this number and multiplying by the detector area and exposure time, and the the energy of a photon, $\frac{\lambda}{hc}$, gives the number of photons at each wavelength incident onto the detector. The detectivity of the spectrometer is found by dividing this photon density by the counts recorded by the spectrometer.

A secondary calibration measurement was done using a blackbody spectrum. The blackbody was turned on approximately four hours before testing to allow for equilibration to occur, well more than the time estimated in the instructions. It was set to 1,350 K to allow for as much intensity in the shorter wavelengths as possible. The spectrometer has two grating options, one maximaized for 750 nm and the other for 300 nm. Moving the fiber closer to the blackbody at the grating switch was done to again maximize the output in the blue. The detector was held at a distance of 20.9 cm from the blackbody when calibrating the 750 nm grating and 6.6 cm for the other. At both of these distances, it can be assumed that the light is emitted from a Lambertian disk. The spectral irradiance emitted from a Lambertian disk is given by:

$$I = \frac{2hc^2}{\lambda^5} \frac{1}{e^{\frac{hc}{\lambda kT}} - 1} \pi \frac{l^2}{l^2 + R^2}.$$

Here T is the temperature in Kelvin, R is the distance from the disk, l is the distance from the center, both in meters, and k is Boltzmann's constant (7). From here it is the same analysis as that for the halogen lamp. Fig. 18 shows the spectroscopic detectivity found using both methods. The two graphs are normalized to their value at 780 nm. An absolute calibration is not needed as only trends in the data are analyzed. The normalized graphs show a very good agreement for our relative calibration. The changing of the grating accounts for the large discontinuity around 575 nm. Even with the attempt to maximize the intensity of the blackbody at all wavelengths, the spectrum emitted in the near UV portion was very small, which can account for the incongruities between the quartz halogen calibration and this one.

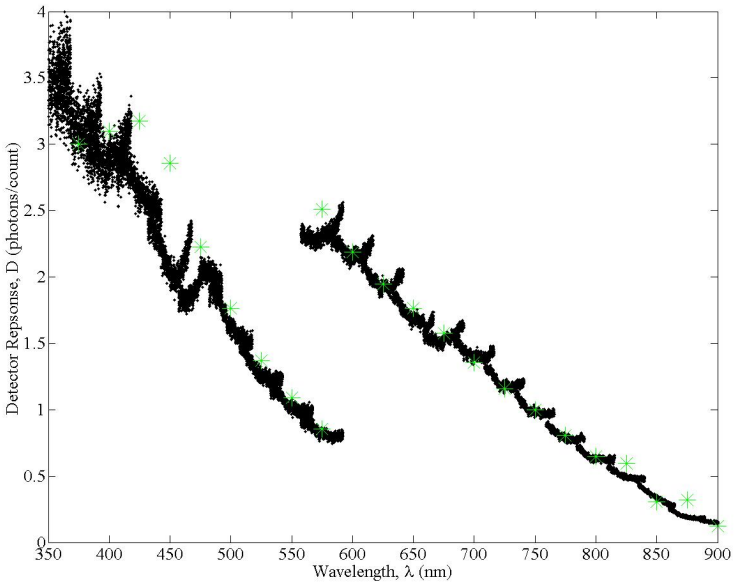

Figure 18. The black points are those from the halogen lamp, the blue points are that of the blackbody, and the red are the theoretical quantum efficiency calculated from the manufacturers. The difference between multiple sources of calibration grow in the shorter wavelengths due to the small signal of the blackbody in this spectral region.

The final check of the detectivity measurements was done by finding the manufacturers quoted specifications for the quantum efficiency of the Princeton Instruments CCD Camera and the reflectivity efficiency of the two gratings. The plots of these

values were taken from Princeton Instruments and Acton's websites, respectively. A MATLAB digitizer was used to pull numbers off of the plots, so this only serves as an estimate of the probable detector response. They, can be found on Fig 18, and are in good agreement with the rest of the data.

Appendix B. Thermal Equilibrium

To motivate the decision to investigate the steady state solution of the rate equations, an appeal to thermodynamics is implemented. If the kinetics were neglected for just a moment, if the rubidium was able to reach thermodynamic equilibrium in the cell then it should be obvious why a steady state solution is justified. If thermodynamic equilibrium is reached, the rubidium density as a function of energy is constant and therefore the density of a given energy level is as well. A Boltzmann distrobution is expected once equilibrium is reached. The functional form of a Boltzmann distribution looks like $n(E_i) \propto g_i e^{\frac{E_i}{kT}}$, where $n(E_i)$ is the density of rubidium at some energy level E_i, g_i is the degeneracy of of that energy level, k is the Boltzmann constant. T is not the temperature of the cell, it is instead an apparent electronic temperature. It does not have any physical meaning, except that it describes how energetic the electrons really are.

To investigate the possibility of thermal equilibrium, a similar set up was used as described in the Chapter III. The primary difference was that instead of a homemade cell, a Triad rubidium cell was used. To ensure the findings were valid over the entire range of pressures, this investigation was done at vacuum. Collisions tend to drive systems toward equilibrium, so if equilibrium is found at vacuum, then as you increase buffer gas pressure—and therefore collisional frequency—thermodynamic equilibrium will be reached faster.

Radiation trapping must be considered again here, and it will be approached a bit differently in this case. Molisch and Oehry introduce an escape factor in (18) that is a function solely of absorbence. This escape factor acts a probability that a photon emitted at the center of the cell is able to reach to cell wall and escape to the detector. There are a few reasons this much simpler escape factor approach is not used in the earlier work. Primarily, the assumptions made to derive the escape factor may not

be fully valid in the experiment. It will definitely give the general picture of radiation trapping as it is occurring, enough to investigate the thermodynamic equilibrium, but to the escape factor approach any further would be leaving out much of the physics. For instance, the functional form for the escape factor assumes a Doppler broadened line. This is almost assured in buffer pressures near zero, but quickly becomes false, as helium is increased. The function form of the trapping factor for a Doppler broadened line, in a infinite cylinder, with high opacity is given as:

$$\bar{\eta} \approx \frac{2}{\sigma n l}\sqrt{\frac{\ln(\sigma n l)}{\pi}} \tag{25}$$

Here σ is the absorption cross section of a transition, n is the rubidium density in the lower state of the transition, and l is radius of the cell (18). The only assumption needed to justify the infinite cylinder simplification is that the cylinder length is longer than its diameter, which is the case in this set-up. The only assumption needed to justify the high opacity remark is for $\sigma n l$ to be much greater than one, which it most assuredly is in all cases.

The only transitions that were assumed to be undergoing trapping were ones that ended in the ground state. While it is true that in the volume illuminated by the pump beam the densities of the some excited states, specifically the 5P manifold, are comparable to that of the ground state; outside of that relatively small region of the total cell volume the excited density is negligible to that of the ground state rubidium. Because of this, if a photon from a transition that does not terminate on the ground state is able to escape from the beam radius—which is much smaller than the cell radius—it will most likely reach the cell wall, and so it will be said that the escape factor for these transitions is approximately 1.

It has been stated previously that $n_i \propto \frac{I_i}{D_i \xi_i A_i}$, and using this with Eq. 25 it can

be concluded that

$$\ln \frac{I_i}{D_i \xi_i A_i g_i} \propto \frac{-E_i}{kT} \tag{26}$$

If the cell can be believed to be in thermodynamic equilibrium then the electronic temperature can be extracted from the line comparing the energy levels of the upper state and the natural log of the density in that excited state. The results from this experiment done at $235°C$ are displayed in Fig. 19. In this graph, the open circles are the values of the density before trapping and the solid dots are the values after the escape factor was included. The simplistic form for trapping makes the linear regression much stronger.

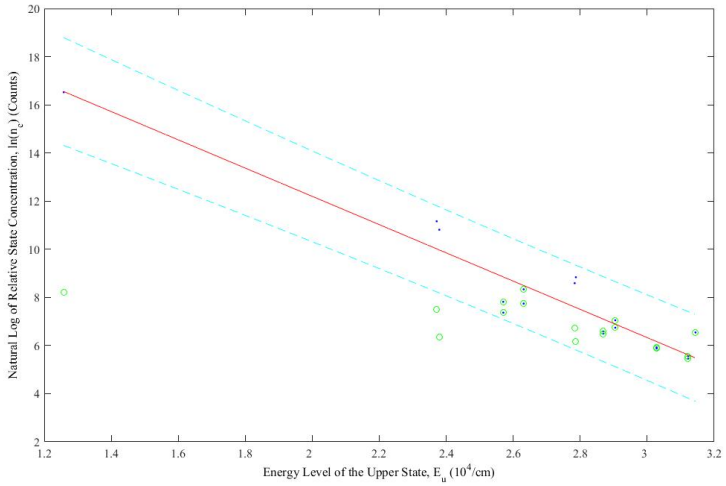

Figure 19. Sample determination of electronic temperature, at $235°C$. The green circles represent as it was produced by the experiment. The blue dots are the values after a naive trapping approach was concluded. The red line is the line fit through the data, whose slope is a function of the electronic temperature. The cyan dashed line represents the error bound for the fit. They were found using the regression statistics and represent a 95% confidence interval.

The electronic temperature's dependence on the true cell temperature is shown in Fig. 20. The rubidium in the cell reaches the same electronic temperature regardless of cell temperature. This seems to be counter intuitive but it is not. The cell temperature will increase the average speed of a rubidium atom but will do nothing to

increase the energy the electron has. As cell temperature is increased, the population in each energy level tends to increase, but the trend of the Boltzmann plot stayed the same.

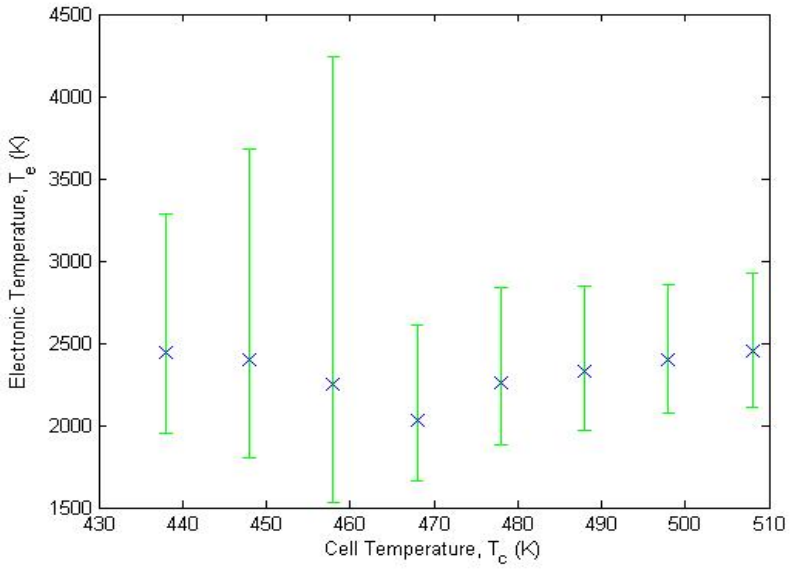

Figure 20. Electronic temperature at increasing cell temperature. The error bars come from the regression statistics and represent a 95% confidence interval.

This constant electronic temperature derived implies that the cell is able to reach this thermodynamic equilibrium between laser pulses. If it was not able to, some rubidium density dependency would be expected. So this Boltzmann approach has shown that the investigation of the steady state solution is a valid way to probe the data. Furthermore, this data shows the necessity of including a correction for radiation trapping for these experiments. Even a overly simplified trapping factor increased the correlation of the data significantly, so it must be carefully considered.

Bibliography

1. P Albers, E Stark, and G Huber. Continuous-wave laser operation and quantum efficiency of titanium-doped sapphire. *JOSA B*, 3(1):134–139, 1986.

2. CB Alcock, VP Itkin, and MK Horrigan. Vapour pressure equations for the metallic elements: 298–2500k. *Canadian Metallurgical Quarterly*, 23(3):309–313, 1984.

3. RV Ambartzumian, NP Furzikov, VS Letokhov, and AA Puretsky. Measuring photoionization cross-sections of excited atomic states. *Applied Physics*, 9(4):335–337, 1976.

4. SA Bakhramov, EV Vaganov, AM Kokhkharov, and OR Parpiev. Laser-induced resonant multiphoton and collisional ionizations of rubidium atoms. In *XVII International Conference on Coherent and Nonlinear Optics (ICONO 2001)*, pages 205–210. International Society for Optics and Photonics, 2002.

5. BD Barmashenko, S Rosenwaks, and MC Heaven. Static diode pumped alkali lasers: model calculations of the effects of heating, ionization, high electronic excitation and chemical reactions. *Optics Communications*, 292:123–125, 2013.

6. RJ Beach, WF Krupke, VK Kanz, SA Payne, MA Dubinskii, and LD Merkle. End-pumped continuous-wave alkali vapor lasers: experiment, model, and power scaling. *JOSA B*, 21(12):2151–2163, 2004.

7. GD Boreman. *Infrared detectors and systems*, volume 24. Wiley-Interscience, 1996.

8. S Chénais, F Druon, S Forget, F Balembois, and P Georges. On thermal effects in solid-state lasers: The case of ytterbium-doped materials. *Progress in Quantum Electronics*, 30(4):89–153, 2006.

9. DP Devor, LG DeShazer, and RC Pastor. Nd: Yag quantum efficiency and related radiative properties. *Quantum Electronics, IEEE Journal of*, 25(8):1863–1873, 1989.

10. L Ge, W Hua, H Wang, Z Yang, and X Xu. Study on photoionization in a rubidium diode-pumped alkali laser gain medium with the optogalvanic method. *Optics Letters*, 38(2):199–201, 2013.

11. EJ Hurd, JC Holtgrave, and GP Perram. Intensity scaling of an optically pumped potassium laser. *Optics Communications*, 357:63–66, 2015.

12. ZJ Jabbour, RK Namiotka, J Huennekens, M Allegrini, S Milošević, and F De Tomasi. Energy-pooling collisions in cesium: 6 p j+ 6 p j→ 6s+ (nl= 7p, 6d, 8s, 4f). *Physical Review A*, 54(2):1372–1384, 1996.

13. RJ Knize, BV Zhdanov, and MK Shaffer. Photoionization in alkali lasers. *Optics Express*, 19(8):7894–7902, 2011.

14. A. Kramida, Yu. Ralchenko, J. Reader, and and NIST ASD Team. NIST Atomic Spectra Database (ver. 5.3), [Online]. Available: `http://physics.nist.gov/asd` [2016, January 11]. National Institute of Standards and Technology, Gaithersburg, MD., 2015.

15. WF Krupke. Diode-pumped alkali laser, November 4 2003. US Patent 6,643,311.

16. WF Krupke. Diode pumped alkali lasers (dpals)a review (rev1). *Progress in Quantum Electronics*, 36(1):4–28, 2012.

17. MA Mahmoud, YEE Gamal, and HA Abd El-Rahman. Ion formation in laser-irradiated cesium vapor. *Journal of Quantitative Spectroscopy and Radiative Transfer*, 102(2):241–250, 2006.

18. AF Molisch and BP Oehry. *Radiation trapping in atomic vapours*. Oxford University Press, 1998.

19. BQ Oliker, JD Haiducek, DA Hostutler, GA Pitz, W Rudolph, and TJ Madden. Simulation of deleterious processes in a static-cell diode pumped alkali laser. In *SPIE Proceedings*, pages 89620B–89620B. International Society for Optics and Photonics, 2014.

20. R Payling, P Larkins, and TJ Vickers. Optical emission lines of the elements. *Applied Spectroscopy*, 55:295–296, 2001.

21. P Rabinowitz, S Jacobs, and G Gould. Continuous optically pumped cs laser. *Applied Optics*, 1(4):513–516, 1962.

22. AD Sharma, HA Schuessler, and RH Hill Jr. Laser-induced-fluorescence detection of collisional excitation transfer in atomic rubidium vapor during collisions with noble-gas and rubidium atoms. *Physical Review A*, 37(12):4649–4655, 1988.

23. CV Sulham, GP Perram, MP Wilkinson, and DA Hostutler. A pulsed, optically-pumped rubidium laser at high pump intensity. *Optics Communications*, 283(21):4328–4332, 2010.

24. CV Sulham, GA Pitz, and GP Perram. Blue and infrared stimulated emission from alkali vapors pumped through two-photon absorption. *Applied Physics B*, 101(1-2):57–63, 2010.

25. CE Theodosiou. Lifetimes of alkali-metalatom rydberg states. *Physical Review A*, 30(6):2881–2909, 1984.

26. S Wane. Radiative recombination in rubidium. *Journal of Physics B: Atomic and Molecular Physics*, 18(19):3881–3893, 1985.

27. S Yi-Fan, D Kang, M Bao-Xia, W Shu-Ying, and C Xiu-Hua. Energy-pooling collisions in rubidium: $5p_{3/2} + 5p_(3/2) \rightarrow 5s + (nl = 5d, 7s)$. *Chinese Physics Letters*, 22(11):2805–2808, 2005.

28. ND Zameroski, W Rudolph, GD Hager, and DA Hostutler. A study of collisional quenching and radiation-trapping kinetics for rb (5p) in the presence of methane and ethane using time-resolved fluorescence. *Journal of Physics B: Atomic, Molecular and Optical Physics*, 42(24):245401–245410, 2009.

29. BV Zhdanov and RJ Knize. Review of alkali laser research and development. *Optical Engineering*, 52(2):021010–021010, 2013.

30. BV Zhdanov, MD Rotondaro, MK Shaffer, and RJ Knize. Power degradation due to thermal effects in potassium diode pumped alkali laser. *Optics Communications*, 341:97–100, 2015.

31. J Zweiback and WF Krupke. 28w average power hydrocarbon-free rubidium diode pumped alkali laser. *Optics Express*, 18(2):1444–1449, 2010.

REPORT DOCUMENTATION PAGE

Form Approved
OMB No. 0704–0188

1. REPORT DATE *(DD–MM–YYYY)*	2. REPORT TYPE	3. DATES COVERED *(From — To)*
24–03–2016	Master's Thesis	Sept 2014 — Mar 2016

4. TITLE AND SUBTITLE

Kinetics of higher lying Rb states after,
Pulsed excitation of the D_2 transition
in the Presence of Helium

5a. CONTRACT NUMBER

5b. GRANT NUMBER

5c. PROGRAM ELEMENT NUMBER

6. AUTHOR(S)

Wallerstein, Austin J 1Lt, USAF

5d. PROJECT NUMBER

5e. TASK NUMBER

5f. WORK UNIT NUMBER

7. PERFORMING ORGANIZATION NAME(S) AND ADDRESS(ES)

Air Force Institute of Technology
Graduate School of Engineering and Management (AFIT/EN)
2950 Hobson Way
WPAFB OH 45433-7765

8. PERFORMING ORGANIZATION REPORT NUMBER

AFIT-ENP-MS-16-M-087

9. SPONSORING / MONITORING AGENCY NAME(S) AND ADDRESS(ES)

Patricia Wallentine
Missle Defense Agency
Bldg 5222 Martin Road
Redstone Arsenal AL 35898-0001
Email:Patricia.Wallentine@mda.mil

10. SPONSOR/MONITOR'S ACRONYM(S)

MDA/DVL

11. SPONSOR/MONITOR'S REPORT NUMBER(S)

12. DISTRIBUTION / AVAILABILITY STATEMENT

DISTRIBUTION STATEMENT A:
APPROVED FOR PUBLIC RELEASE; DISTRIBUTION UNLIMITED.

13. SUPPLEMENTARY NOTES

This material is declared a work of the U.S. Government and is not subject to copyright protection in the United States.

14. ABSTRACT

The Diode Pumped Alkali Laser (DPAL) is a high power, three-level laser system that employs diode bars to optically excite an alkali metal vapor. It lases along the D_1 transition, between the two lowest energy levels, ${}^2P_{\frac{1}{2}}$ and ${}^2S_{\frac{1}{2}}$. Higher lying energy states are produced at higher population density via energy pooling and multiphoton processes. Pulsed laser excitation of rubidium at approximately 1 MW/cm^2 has been studied at helium pressure up to 900 Torr. Emissions from energy states as high as 82D suggests modest ionization, though these intensities decrease drastically at buffer gas pressures above 250 Torr. Blue emission from the $6^2P \rightarrow 5^2S_{\frac{1}{2}}$ transition and red emission from the $5^2D \rightarrow 5^2P$ transition indicate population in these upper states that persists at all helium pressures used in this experiment. A basic kinetic model was created to describe the concentration at these higher lying states. Optical trapping is severe at temperatures above 450 K. Diffusion of the rubidium is very slow, requiring mixing times exceed 45 minutes.

15. SUBJECT TERMS

Diode Pumped Alkali Laser, Alkali, Ionization

16. SECURITY CLASSIFICATION OF:			17. LIMITATION OF ABSTRACT	18. NUMBER OF PAGES	19a. NAME OF RESPONSIBLE PERSON
a. REPORT	b. ABSTRACT	c. THIS PAGE			Dr. Glen P. Perram, AFIT/ENP
U	U	U	U	62	19b. TELEPHONE NUMBER *(include area code)* (937) 255-3636, x4504; glen.perram@afit.edu